Acoustic impedance inversion and CO_2 flood detection at the Alder Flats ECBM project

Jason M. McCrank and Don C. Lawton

ABSTRACT

The 3D post-stack vertical component data from the Alder Flats site were inverted to estimate the acoustic impedance of the Upper and Lower Ardley coal zones. The theory of two methods of inverting the data, a model-based algorithm and a constrained sparse spike algorithm, is reviewed. The inversion with each of the algorithms shows a similar result. While the band-limited nature of the seismic data and the resulting inversion does not resolve each sub-zone of the Ardley Coals, the parameter estimation appears to be accurate and unbiased. Both inversions show a low acoustic impedance anomaly approximate areal extent of 1300 – 1800 m^2 to the northeast of a well that was used to inject 180 tonnes of CO_2 into one of the sub-zone coals of the Ardley Coal zone prior to acquisition of the seismic survey. Gassmann modelling shows that a simple fluid substitution of formation water for gaseous CO_2 could explain the degree of anomaly seen, however, other interpretations are possible.

INTRODUCTION

A 3D vertical component seismic survey was acquired by the University of Calgary at the Alder Flats site in June of 2007 (discussed in McCrank and Lawton, 2007). The field layout (FIG. 1) was approximately 560 x 560 m. There are two wells within the survey limits but only well 102/7-28 had quality sonic and density logs and is the only well analyzed in this paper. However, because the total depth of the 102/7-28 well only extended to 485 m, additional well data was spliced onto the bottom of the 102/7-28 well log from a regional well.

The survey was intended to image the stratigraphy of the Ardley Coal Zone which is illustrated in the well correlation cross-section shown in FIG. 2. The Ardley Coal Zone is informally broken into the Upper and Lower Ardley coal zones. The Upper Ardley is an approximately ~10 m gross thickness coal zone and the Lower Ardley coal zone is represented by two smaller zones which are the Mynheer coal zone and the Silkstone coal zone. The Mynheer coals are the deepest sub-zone of the Lower Ardley coal zone and represent ~8 m in gross coal thickness while the Silkstone coals are ~3 m in gross coal thickness.

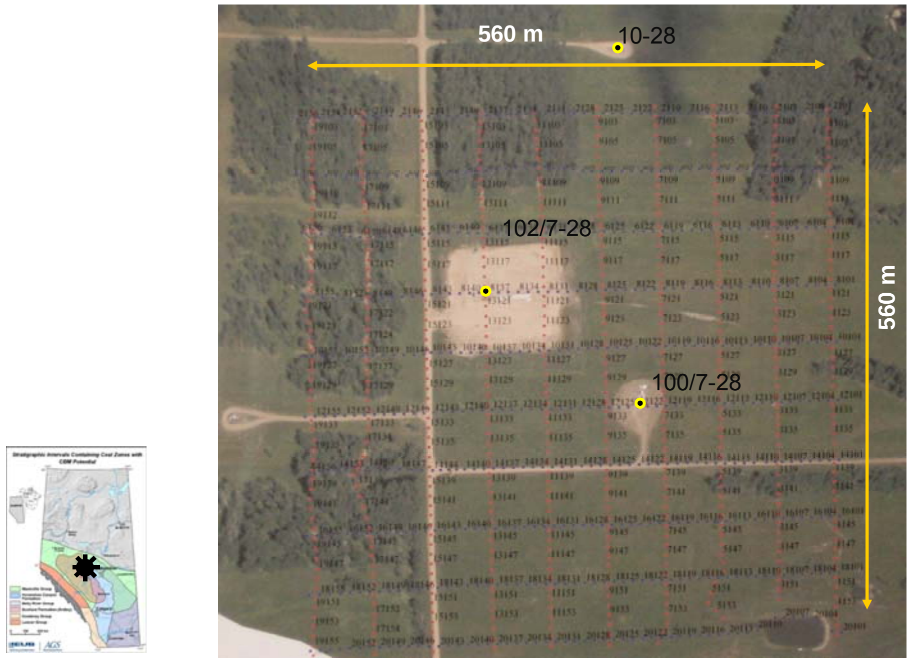

FIG. 1. Survey field layout and well locations.

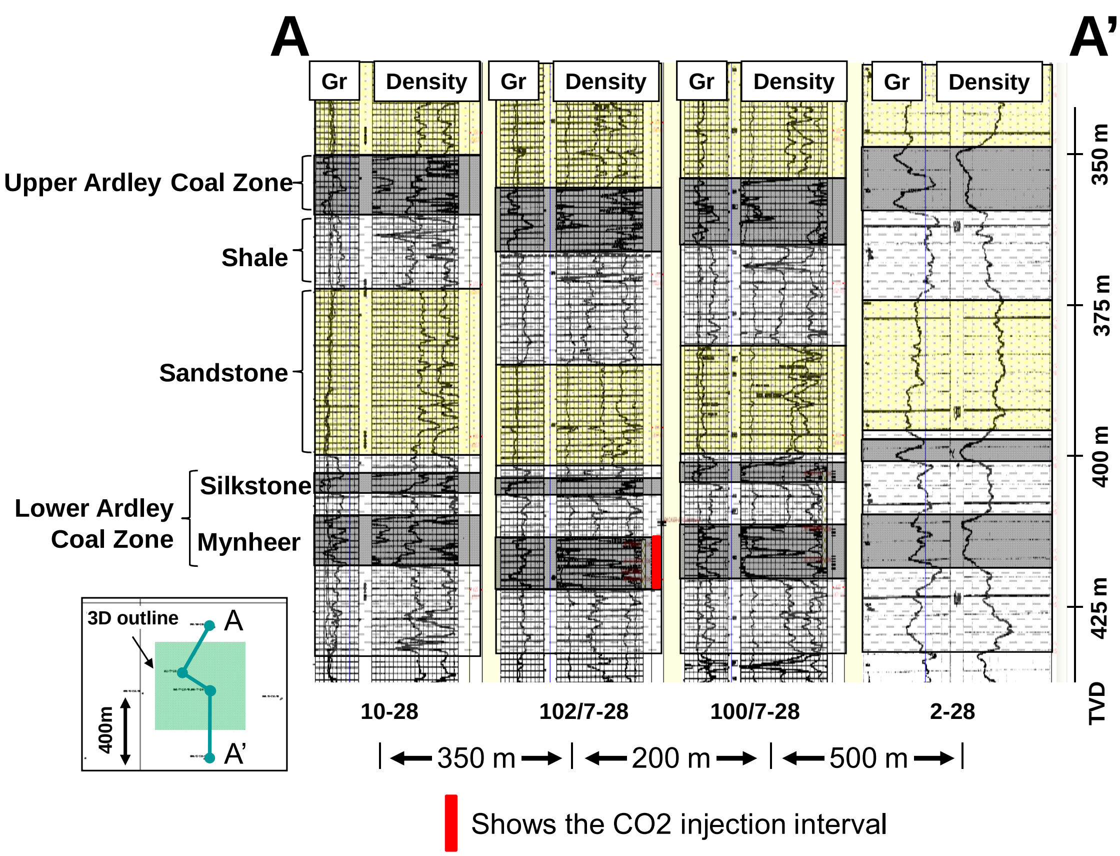

FIG. 2. A N-S geological cross-section showing the sub-zones of the Ardley Coal Zone. CO_2 injection was into the Mynheer coal zone. (Log display courtesy of IHS Energy Accumap).

Prior to the time of the seismic survey, 180 tonnes of CO_2 was injected through the 102/7-28 well into the Mynheer coal zone for the purposes of enhanced coalbed methane production and carbon sequestration. Under injection pressure, the CO_2 would have entered the coals in a liquid state but quickly flashed to a gaseous state under reservoir conditions. It is believed that the CO_2 would have moved first through the macro-porosity cleat (fracture) system of the coals and then entered the coal's meso- and micro- porosity through a diffusion process. CO_2 has been shown to be an organic solvent in laboratory experiments, and because a coal's matrix is an organic material, it has been shown to reduce the elastic moduli of the coal matrix (Day et al., 2007; Karacan, 2007; Khan and Jenkins, 1985; Larsen, 2004; Levy et al., 1997; Shimada et al., 2005; Viete and Ranjith, 2006; Viete and Ranjith, 2007). However, experimental data is terse and general predictions for various pressure, temperature and coal types have not been published.The Alder Flats data were inverted to estimate acoustic impedance in an attempt to detect a signature of the injected CO_2.

The Utility of Acoustic Impedance Inversion

Acoustic impedance (Z_p, Z or AI) is defined as the product of compressional wave velocity (v_p) and density (ρ):

$$Z = v_p \times \rho \quad .$$

Because both velocity and density are indicators of lithology, fluid content, porosity and other petrophysical properties, a quantitative estimate of acoustic impedance from seismic data can be used to characterize petrophysical properties of the subsurface. If a seismic trace is treated as a band-limited estimate of the earth's layered normal incidence reflectivity, the trace only gives information about the boundary between layers, not the layers themselves. However, since the normal incidence reflection coefficient (r_i) at the i^{th} interface of two layers is given by:

$$r_i = \frac{Z_{i+1} - Z_i}{Z_{i+1} + Z_i} \tag{1}$$

the data from a seismic trace can be used to give an acoustic impedance estimate of the reflecting layers.

Inversion estimates of acoustic impedance provide several advantages over interpretation of the stacked traces themselves (Latimer et al., 2000; Veeken and Da Silva, 2004):

- Acoustic impedance inversions incorporate well log information into the parameter estimate which includes low frequency information that is not available in the seismic data alone.
- In estimating acoustic impedance of a layer, an attempt to remove the wavelet is made which can reduce wavelet side lobe and tuning effects.
- Seismic data is a band-limited estimation of the reflectivity at the interface between layers, while an acoustic impedance estimate, although also band-limited, is a property of the rock layers themselves.

- The layer based acoustic impedance rock property is more easily correlated with well data which is also layer based information (as opposed to layer interface information).
- Because acoustic impedance is a rock property, it can be more easily related to other petrophysical properties such as fluid content and porosity.

Although there are other types of impedance (i.e. shear, elastic, etc.), the remainder of this paper only discusses acoustic impedance. For the sake of brevity "acoustic impedance" is shortened to "impedance".

METHODS OF INVERSION

Multiple methods of inverting post-stack seismic traces to find impedance have been developed. Russell and Hampson (1991) reviewed the band-limited method, the model based method, and the sparse spike method and showed that each has its advantages and disadvantages.

Band-limited Inversion

The band-limited method was first proposed by Lindseth (1979). Normal incidence reflectivity at a boundary interface is given as by Equation-1 which can be rearranged to give:

$$Z_{i+1} = Z_1 \prod_{j=1}^{i} \left(\frac{1+r_j}{1-r_j} \right) \tag{2}$$

where r_i is the reflection coefficient at the i^{th} interface and Z_i is the impedance of the i^{th} layer. Thus if the impedance of the first layer is known and the reflection coefficients of the subsequent layers are known, the impedance of any layer can be estimated. Treating the seismic trace as an estimate of the reflectivity, the trace can be inverted to yield an impedance estimate. Another approach to estimating impedance is to use an approximation of Equation-1:

$$r(t) \approx \frac{1}{2} \frac{d[\ln Z(t)]}{dt} \tag{3}$$

Notably, this approximation assumes that $|r| < 0.3$ (Lines and Newrick, 2004). Equation-3 can be rearranged to give:

$$Z(t) = Z(0) \exp\left[2 \int_0^t r(u)du \right] \tag{4}$$

and again the impedance can be estimated from the reflection series alone if Z(0) is known. In recognition that the seismic trace lacks content at the low end of the frequency spectrum, the low frequency trend is introduced into the solution by adding the low frequency high-cut filtered impedance estimate from regional well data. The advantage of the band-limited inversion method is its simplicity. The principal disadvantage is that it does not account for the wavelet embedded in the seismic trace.

Model-based Inversion

Improved impedance inversions incorporate information about the wavelet. One of the Hampson Russell Software (HRS) inversion methods is a model-based inversion. Cooke and Schneider (1983) were the first to use such a method to solve for acoustic impedance from poststack seismic data. In general, the method uses an initial guess model of the impedance which is used in an objective function that includes consideration of the extracted wavelet. The initial model incorporates low frequency information from local wells. The objective function is minimized by iterative perturbation of the model which results in a reasonable solution if the initial guess is within the region of global convergence of the objective function.

The HRS technique is a highly evolved method that minimizes the following objective function (HRS Strata Theory): $\mathbf{e} = (\mathbf{T} - \mathbf{wDL})$ (5)

where **e** is the residual difference (in vector notation) between the seismic trace **T** and the trace resulting from the model data, **wDL**, where **w** is the convolutional wavelet matrix for an *n* sample wavelet:

$$\mathbf{w} = \begin{bmatrix} w(1) & 0 & \cdots \\ w(2) & w(1) & \ldots \\ \vdots & w(2) & \ldots \\ w(n) & \vdots & \ldots \\ 0 & w(n) & \ldots \\ \vdots & 0 & \\ 0 & \vdots & \ddots \end{bmatrix}$$

L is a vector consisting of the logarithm of impedance for *m* model samples:

$$\mathbf{L} = \begin{bmatrix} L(1) \\ L(2) \\ \vdots \\ L(m) \end{bmatrix}$$

where L(i) = log (Z(i)), and Z(i) is the impedance model,
and **D** is an *m*-1 by *m* derivative matrix where m is the number of layers to be solved for and *m*-1 is the number of reflection coefficients, given as:

$$\mathbf{D} = \frac{1}{2}\begin{bmatrix} -1 & 1 & 0 & 0 & 0 & \ldots \\ 0 & -1 & 1 & 0 & 0 & \cdots \\ 0 & 0 & -1 & 1 & 0 & \ldots \\ \vdots & & & & & \ddots \end{bmatrix}$$

The sum of the square of the errors is given by:

$$\mathbf{e}^T\mathbf{e} = (\mathbf{T} - \mathbf{wDL})^T(\mathbf{T} - \mathbf{wDL}) \tag{6}$$

Using linear inverse theory (see Aster et al., 2005), minimizing $\mathbf{e}^T\mathbf{e}$ leads to the "normal equation" (with a stabilization factor, a):

$$((\mathbf{D}^T\mathbf{w}^T\mathbf{wD})+a\mathbf{I})\mathbf{L} = \mathbf{D}^T\mathbf{w}^T\mathbf{T} \tag{7}$$

However, rather than solving Equation-7 directly for **L**, a solution estimate is found by iterative refinement of a guess at the correct model until $\mathbf{e}^T\mathbf{e}$ is minimized. An initial guess model is seeded in Equation-7 for **L** which includes the low frequency trend from regional wells. Conjugant gradient iteration of **L** then minimizes $\mathbf{e}^T\mathbf{e}$. Because the solution to Equation-7 is non-unique (i.e. there are an infinite number of models that can minimize $\mathbf{e}^T\mathbf{e}$), constraints are introduced that restrict the possible solutions. In the HRS "hard-constraints" algorithm, constraints are imposed on the upper and lower bounds for the impedance estimates. The program allows the user to define the bounds as a percentage of the average impedance of the initial guess model.

The HRS theory manual notes that the algorithm has the property that components of the initial guess model that are not resolved by the data tend to be carried through from the initial guess. Thus the low frequency trend, introduced in the initial guess model, is carried through to the final solution because low frequency data is generally not recorded in the seismic data. Also, high frequencies above the seismic band are carried through if they are not filtered away from the model prior to the inversion. Sparsity in the inversion can achieved via the assumption of a finite number of discrete layers within the inversion window.

Sparse Spike Inversion

The generalized linear inversion approach to impedance estimation assumes that the errors (Equation-5) are distributed according to a Gaussian distribution and the method attempts to minimize the L_2-norm given by Equation-6 (the method of least-squares). However, several authors have shown that an optimal deconvolution of the wavelet from a seismic trace is achieved by minimizing an L_1-norm objective function (Levy and Fullagar, 1981). The argument is that the reflectivity of interest in a seismic trace is best modelled as a series of isolated reflectivity spikes embedded in a greater number of low amplitude, noisy spikes. A solution that minimizes an L_1-norm will draw out the fewest layers and only the major layer boundaries. Also, the introduction of the additional knowledge that the reflectivity series is best modelled by a sparse spike train reduces the non-uniqueness problem of the inversion (Oldenburg et al., 1983). The function to be minimized is:

$$J = \sum_{t=0}^{t_{\max}} |r(t)|$$

Oldenburg et al. (1983) demonstrated a method that solved for a sparse reflectivity series, while still modeling the seismic data. The method then used Equation-2 to find the impedance. The solution was also shown to be more accurate in the presence of noise by introducing upper and lower impedance bounds.

Mixed-norm Inversion

Debeye and van Riel (1990) made the argument that the seismic trace should be modelled as a combination of a series of spikes that are distributed according to a sparse distribution and a series of noisy events distributed according to a Gaussian distribution. They claimed that a best estimate of the reflectivity series is a found by minimizing a mixed-norm objective function:

$$J = L_p(\mathbf{r}) + \lambda L_q(\mathbf{T} - \mathbf{wr})$$

where p and q are the number of the norm to be minimized and λ is a weighting factor between the two terms. p is set to 1 to solve for a sparse spike series and q is set to 2 to model the noise as normally distributed events. λ, also called the trade-off parameter, weighs between solving for a sparse spike series and a series that matches the seismic trace as closely as possible in a least squares sense. A large λ value implies a large penalty on the noise term and results in an overestimation of the reflectivity in the data. When using this method of estimating reflectivity, the selection of an appropriate value for λ is essential.

The final L_2-norm term contains residuals which account for random noise, as well as failures of the mathematical model such as the fact that the full stack doesn't equal the normal incidence reflectivity, that the convolutional model doesn't truly model the earth's seismic response, that there are errors in the estimated wavelet and other possible discrepancies between the model and reality.

ACOUSTIC IMPEDANCE OF THE ARDLEY COALS

Petrophysics at Well Log Resolution

FIG. 3 shows the cross-plot of impedance and Vp/Vs ratio for the 102/7-28 well logs from 300 – 475 m (KB). The cross-plot space has been divided into regions that delineate coal, sandstone and shale lithologies and FIG. 4 shows the resulting lithology log. Coals are easily identified in a region of low impedance with a cut-off of less than $6.0\text{x}10^6$ $kg/m^3*m/s$. Separation of the siliciclastics into sandstones and shales is less obvious in the cross-plot because the two lithologies overlap, however, the lithology boundaries in FIG. 3 have been selected in order to roughly match the bulk lithology trends shown in FIG. 2.

Notably in FIG. 3, while differentiating sandstones and shales would require an estimation of both impedance and Vp/Vs, coals can be easily identified by the single impedance parameter with the (high) cut-off of $6.0\text{x}10^6$ $kg/m^3*m/s$. Also, because impedance is fundamentally a function of density and wave-velocity, which in turn is a function of bulk modulus, shear modulus and density, the impedance of the coals might be changed by the injection of CO_2 and an impedance estimate might be able to locate coal affected by the injected CO_2.

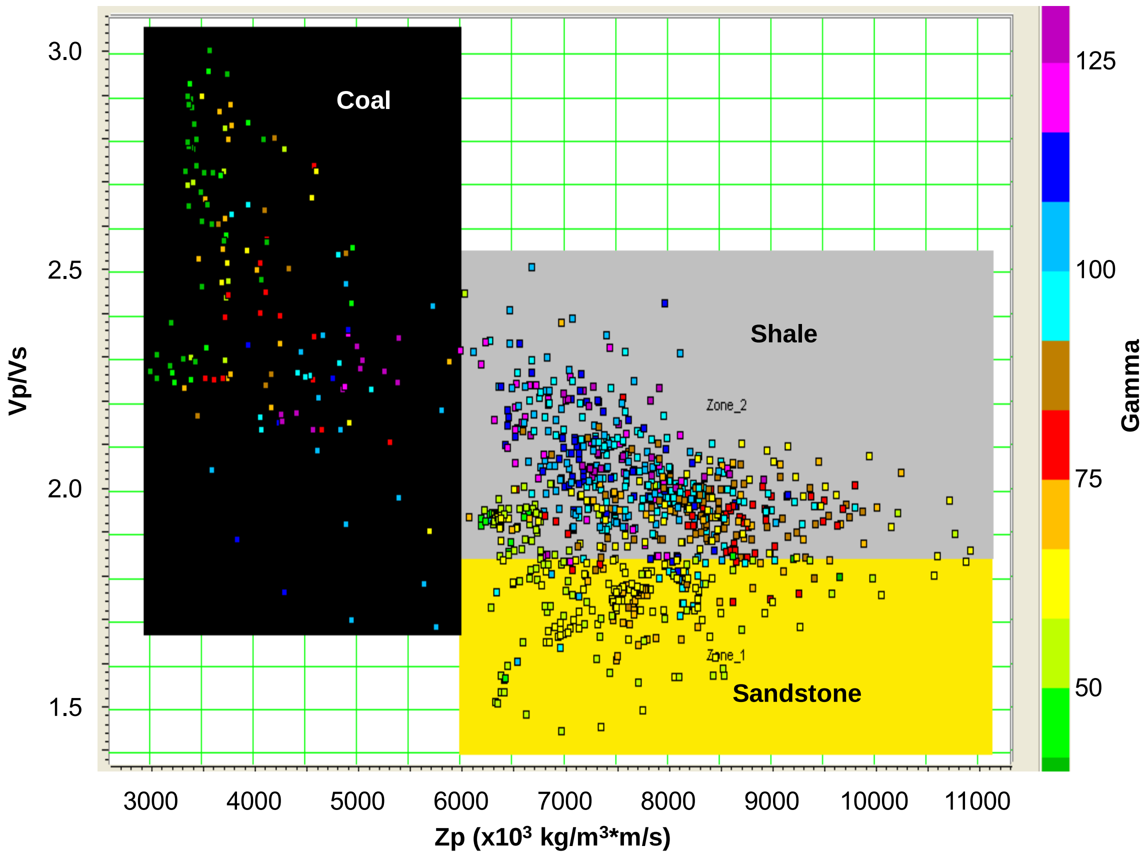

FIG. 3. A cross-plot of impedance and Vp/Vs with gamma values in colour for 102/7-28 from 300 - 475 m (KB). Lithologies are blocked into coals, sandstones and shales in cross-plot space.

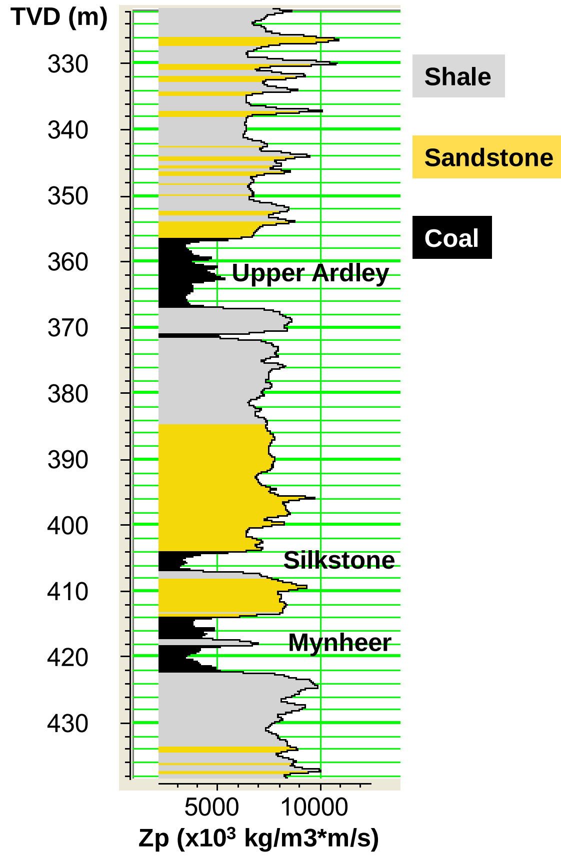

FIG. 4. The lithology log from in the vicinity of the Ardley Coal zone for 102/7-28.

FIG. 3 also shows that within the coal lithology, there is a linear trend with the gamma response. FIG. 5 illustrates this tend in a cross-plot of impedance versus gamma response. The coal lithology follows a trend of increasing impedance with increasing gamma response. The lower impedance, lower gamma zones correspond to the more pure coal lithology and the higher impedance and gamma response indicates shaley coal or coaly shale. The cut-offs are here defined as pure coal with impedance of less than 4.0×10^6 $kg/m^3*m/s$ and shaley coal with a impedance of 4.0×10^6 - 6.0×10^6 $kg/m^3*m/s$. FIG. 6 shows the lithology log with the sub-lithologies of the coal zones delineated. These sub-lithologies of the coal zones can be delineated by impedance, giving a possible hint in terms of interpreting inverted impedance seismic data in coal zones.

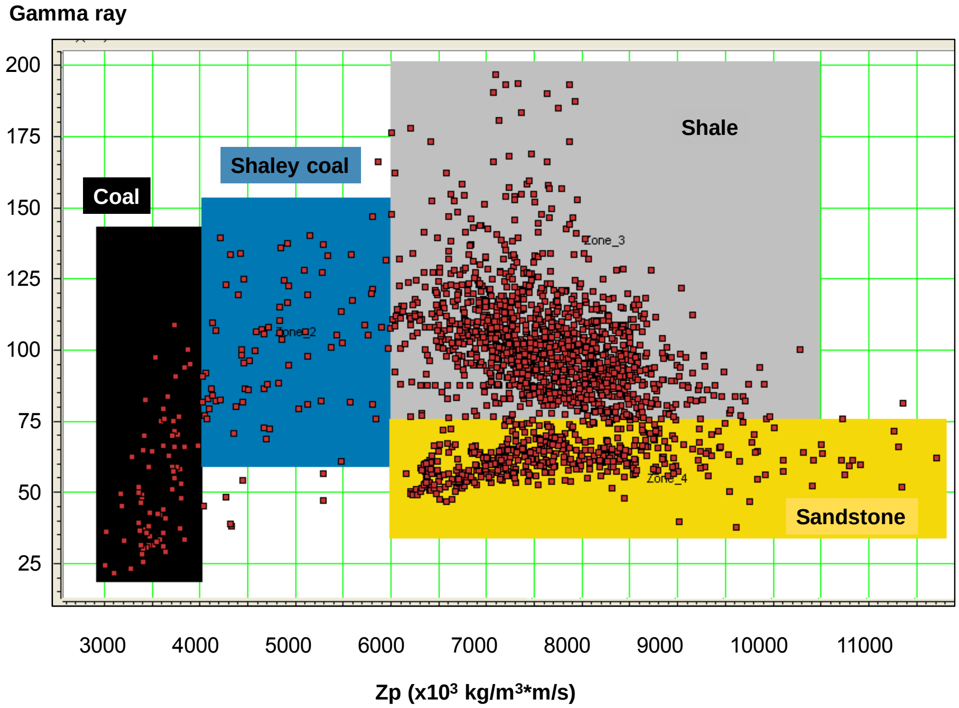

FIG. 5. Cross-plot of impedance and gamma log response from 300 – 475 m (KB) for 102/7-28.

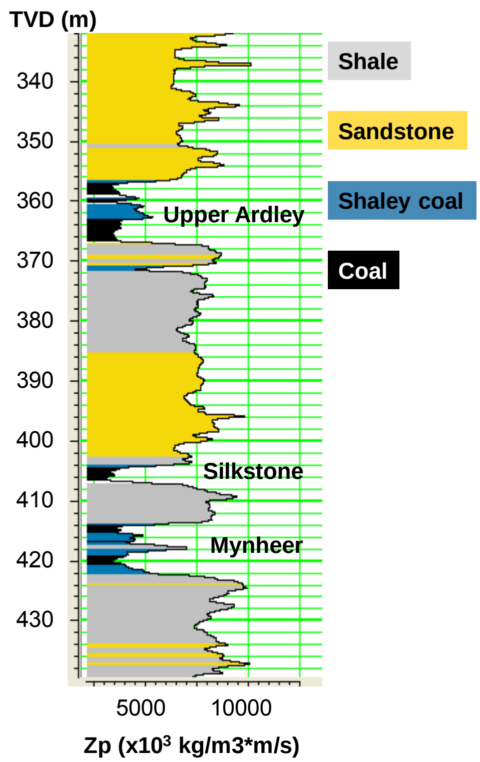

FIG. 6. Lithology log showing the sub-lithologies of coal in the vicinity of the Ardley Coal zone for 102/7-28.

Petrophysics at Seismic Resolution

The lithology log of FIG. 4 has been established using the petrophysical properties acquired at well "logging resolution" (i.e. approximately 15 cm – 1 m scale). However, because seismic data is measured in time and with a limited bandwidth, it is reasonable to expect that lithologies derived from seismic impedance data will have lower resolution than those derived from logs. For example, FIG. 7 shows the same cross-plot as FIG. 5 but at "seismic resolution". The log data have been sampled at 1 ms intervals and have been filtered with a 60 – 70 Hz high cut. Using the same lithology cut-offs as in FIG. 3, FIG. 8 shows the resulting lithology log along with the impedance log at logging resolution and at seismic resolution. There are two significant changes that result with the band-limiting of the impedance. The first is the reduced vertical resolution of thin beds. For example, with the shortened bandwidth, the Mynheer and Silkstone Coal zones are no longer resolved as separate zones. The second significant difference is the reduction in the dynamic range of the impedance estimate. For example, the lowest impedance measured after applying the high cut filter is approximately $4.0x10^6$ kg/m^3*m/s in Upper Ardley Coal zone and approximately $5.0x10^6$ kg/m^3*m/s in the Lower Ardley Coal zone. At logging resolution, the impedance of the purest coals is significantly lower at ~$3.0x10^6$ kg/m^3*m/s.

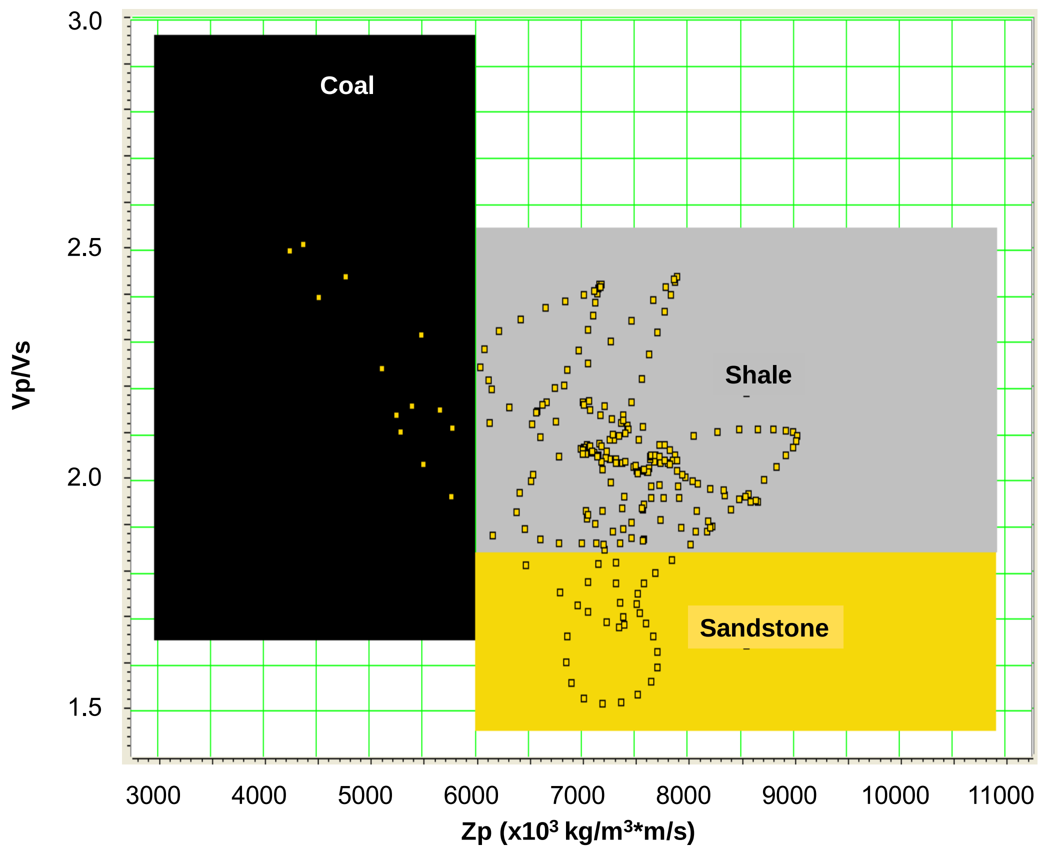

FIG. 7. A cross-plot of impedance and Vp/Vs for 102/7-28 from 300 - 475 m (KB) at 1 ms sampling with a 60 – 70 Hz high cut filter.

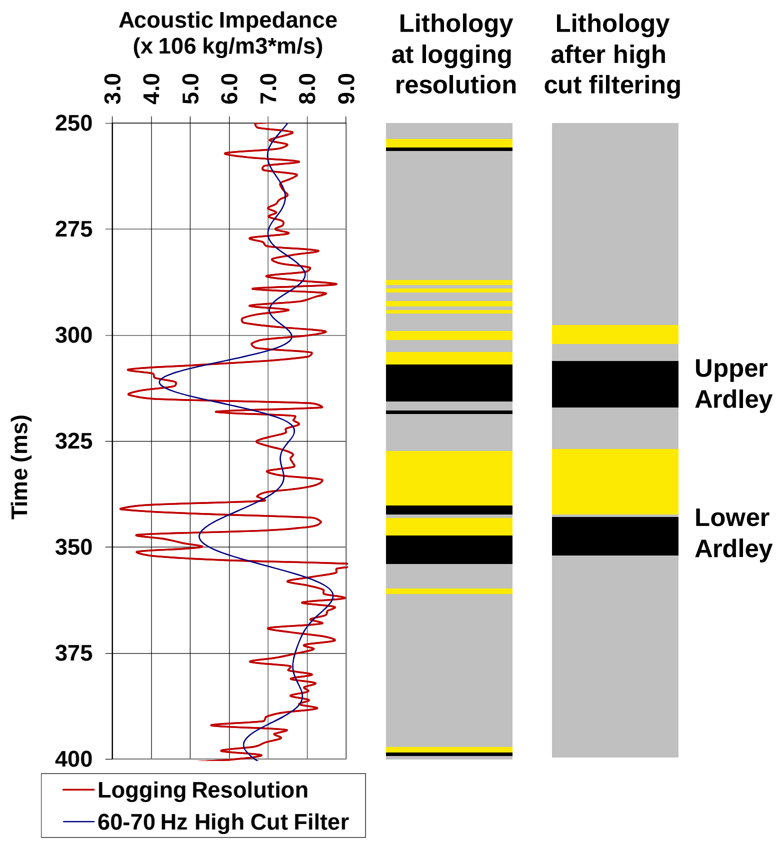

FIG. 8. The impedance log at logging resolution and with a 60 – 70 Hz high cut filter and the corresponding lithology logs: at logging resolution (left) and after high cut filtering (right).

MODEL BASED INVERSION OF THE ALDER FLATS 3D DATA

The workflow for the HRS model-based "hard constraint" inversion method is:

1. Establish the wavelet.
2. Build the initial guess model by interpolating well data throughout the model domain following specified seismic horizons.
3. Low pass filter this initial guess model to the frequency band below the wavelet bandwidth.
4. Test the parameters for the inversion: the pre-whitening value, the number of iterations, the size of the time blocks for the inversion solution, and the bounds for the constraints to be imposed (listed as a percentage of the average impedance of the input initial guess model). Testing is conducted at well locations where the actual impedance values are known and can be compared to the inverted impedance. The parameters are tuned to reduce the residual difference between the logged impedance and the inverted impedance.
5. Run the inversion. The wavelet amplitude is scaled as a part of the inversion process.
6. Inspect the results and the residual difference between the seismic trace and the synthetic that is created with the inverted impedance model.

A 128 ms wavelet was extracted by finding the wavelet that would optimally match the well log reflectivity to seismic at the 102/7-28 well location. The wavelet and the tie to the seismic data are illustrated in FIG. 9. The cross correlation was 0.93 in a window from 180 – 380 ms (where the well log data truly came from the 102/7-28 and not from a regional well).

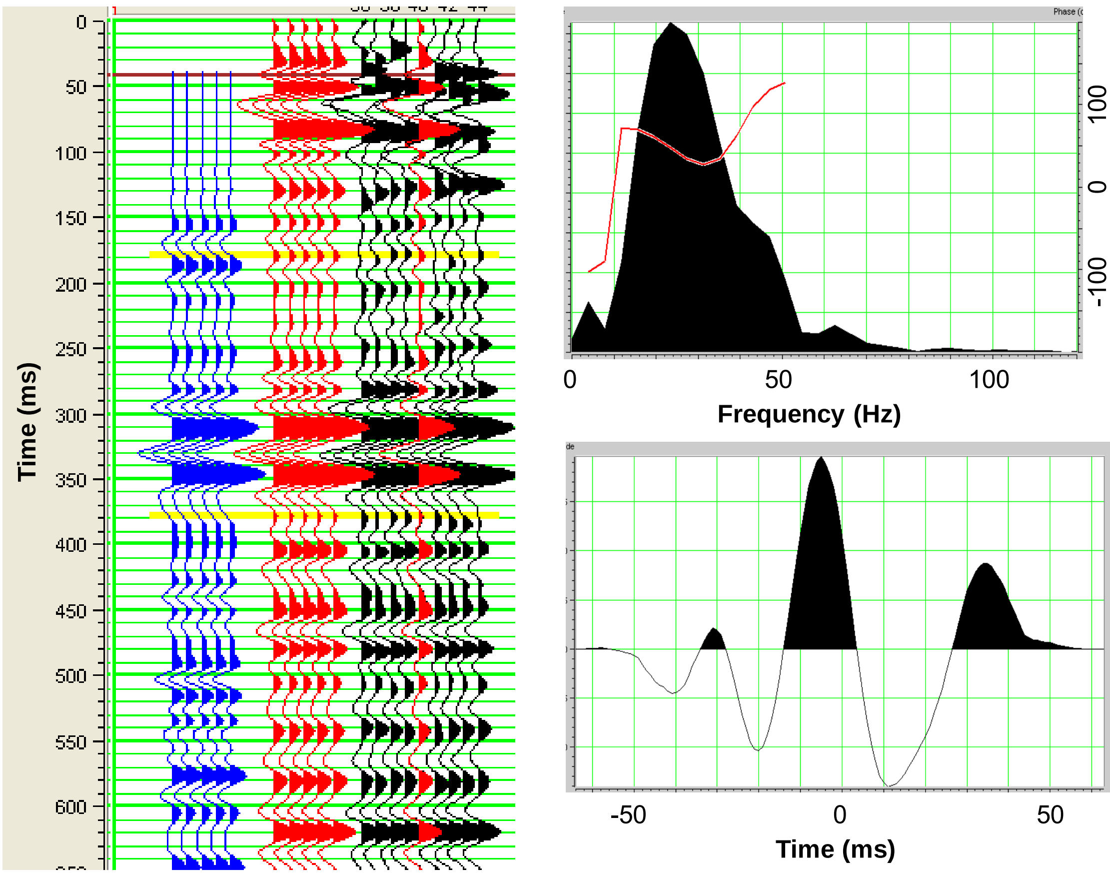

FIG. 9. The wavelet used for the model-based inversion and the synthetic-seismic tie.

Low Frequency Initial Guess Model

The initial guess model was based solely on the calculated impedance at log resolution from the 102/7-28 well. The 102/7-28 well impedance log was extrapolated throughout the survey domain as the initial guess model. In order to account for the geological structure of the domain, the log was extrapolated along the seismic horizon of the Lower Ardley coal zone. Use of a single horizon to guide the extrapolation is believed to give an accurate initial guess model because the stratigraphy is relatively uniform throughout the domain. The initial guess model, at log resolution is illustrated in FIG. 10.

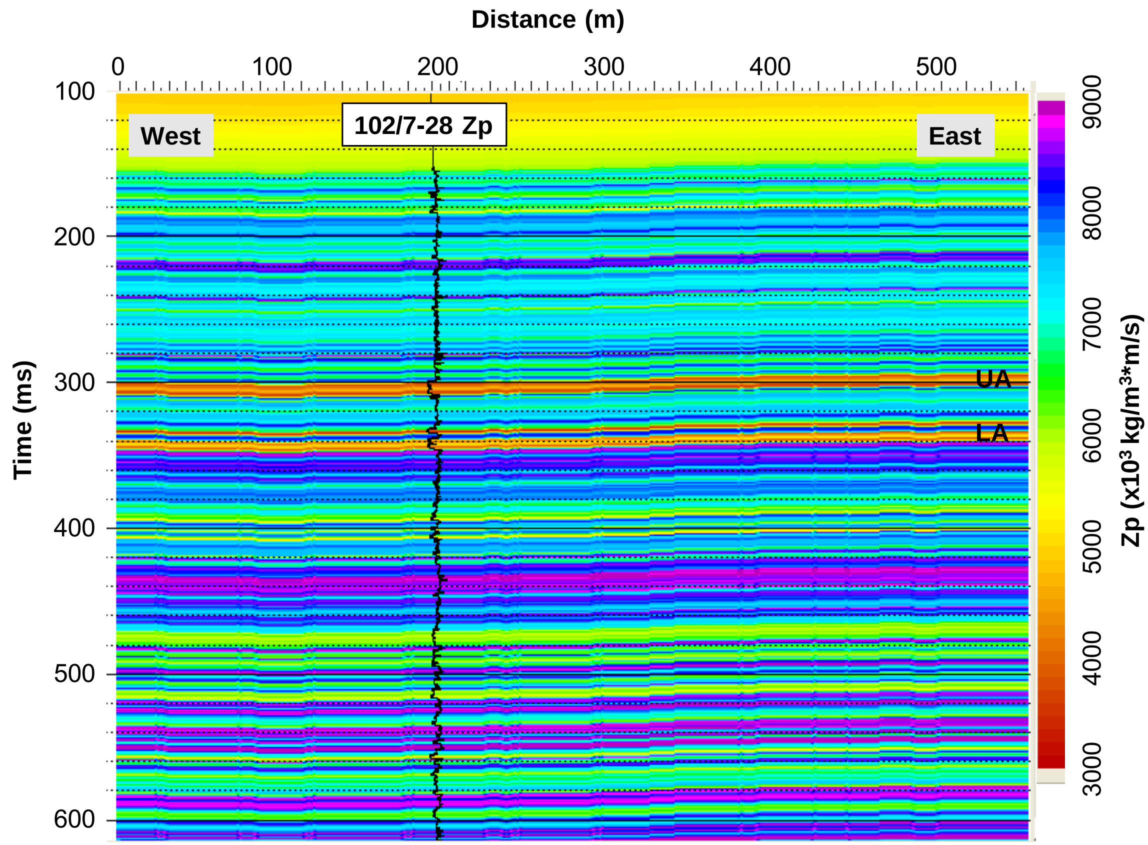

FIG. 10: The initial guess impedance model at log resolution (inline 71).

As noted above, components of the initial guess model that are not resolved by the seismic data are carried through the inversion algorithm. If the model at log resolution was used as the initial guess model, it would be difficult to know what detail in the inverted impedance estimate had come from the data and what had simply been carried through from the initial guess. Therefore, the initial guess was low pass filtered at 10-15 Hz, the frequency band below the band of the seismic data. This low frequency model was used as the initial guess model for the conjugate gradient perturbation of the impedance model. The inversion solution should then minimize the squares of the errors (Equation-6) as long as the low pass filtered initial guess model is within the region of convergence. The low passed initial guess model is illustrated in FIG. 11.

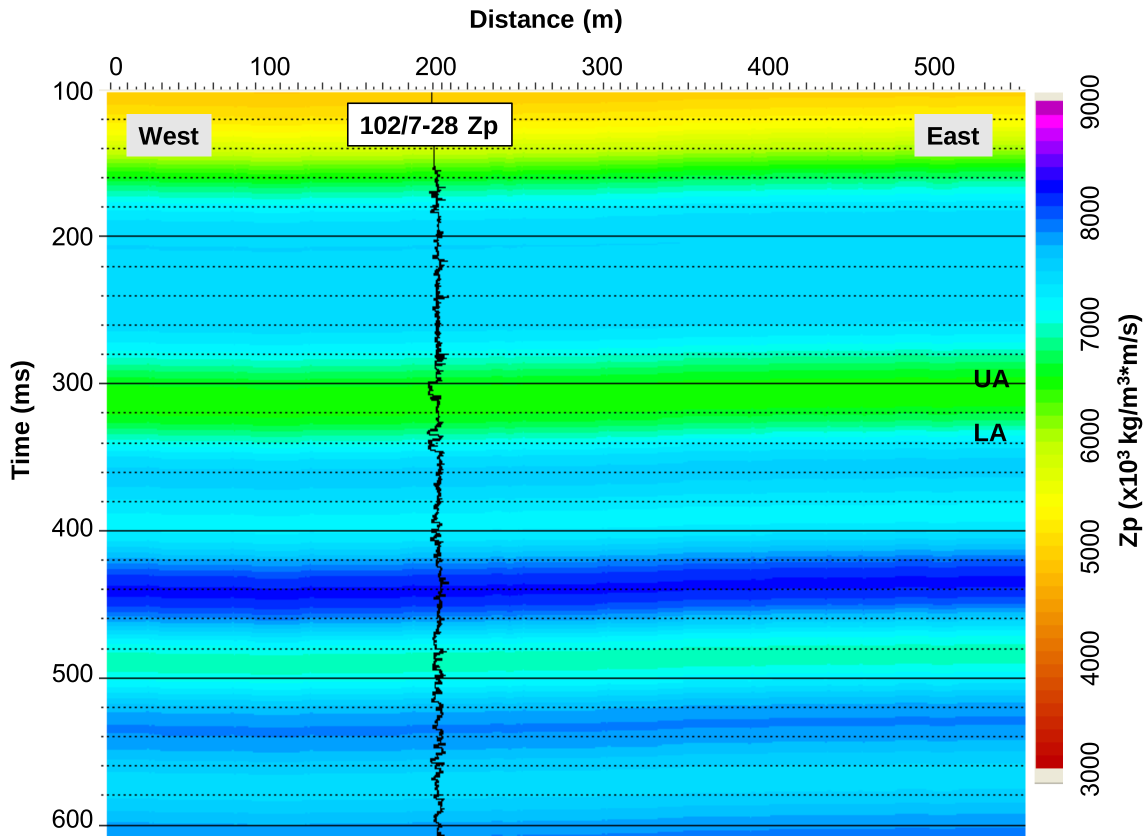

FIG. 11: The initial guess impedance model after low pass filtering 10-15 Hz (inline 71).

Inversion Parameter Testing

The inversion was then run on the traces nearest the 102/7-28 well. The result was compared to the impedance log from the well, and individual parameters were adjusted until the error difference between the log impedance and the inverted impedance was minimized. The parameters were tested in a more or less *ad hoc* way and the elected values are listed in Table 1. The model-based constraint was set to 100% of the average impedance from the initial guess model which is the least constrained setting. Additionally, the inversion was set to invert each trace independently of the other traces.

Table 1. Parameters used in the model-based impedance inversion.

Parameter	Value
Percentage of the average impedance from the initial guess model used as a constraint for the solution impedance.	100%
Block size	1 ms
Stability factor	0.02
Number of iterations	10

The pre-whitening parameter for the inversion was selected by gradually increasing the value until the inverted solution seemed to be stable (i.e. no great change in the error or the inversion trend resulted with further increases in the pre-whitening). The final inverted impedance is compared to the 102/7-28 well impedance log in FIG. 12 and the residual error (difference between the inverted impedance and the well log impedance) and the cross-correlation between the synthetic seismogram of the inverted impedance and the actual seismic trace are listed in Table 2.

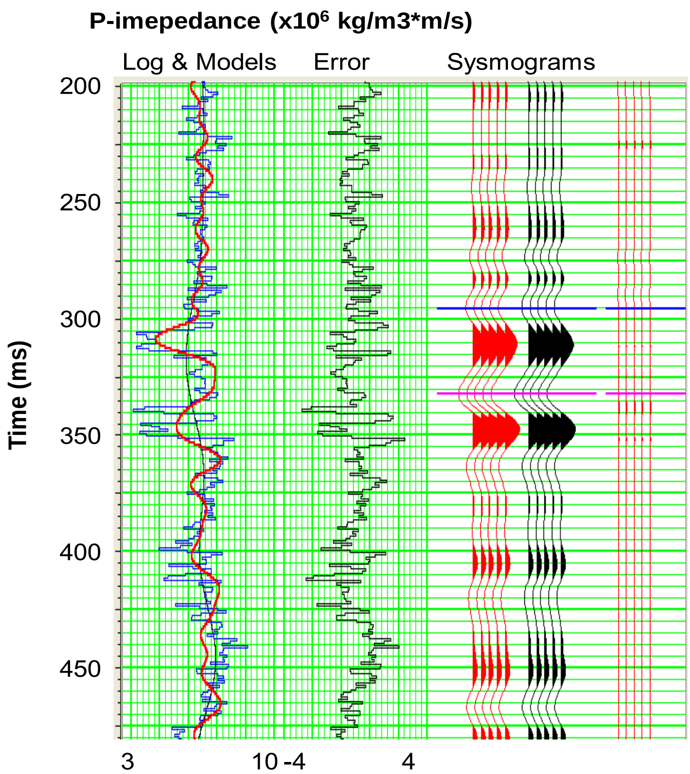

FIG. 12. Analysis of the inverted impedance estimation at the 102/7-28 well location. In the left track, the blue curve is the log impedance, the black curve is the initial guess impedance, and the red trace is the inverted impedance. The middle track black curve is the error in the impedance estimate. On the right, the red seismogram is the synthetic generated from the impedance inversion and the black seismogram is the actual seismic data and the traces on the far right is the difference between the red and black seismograms.

Table 2. The impedance error and synthetic-seismic correlation after impedance inversion at the 102/7-28 well location using the parameters from Table 1 (100-600 ms).

	Value for the match filter wavelet
Impedance error	1018.3
Synthetic-to-data seismogram cross-correlation	0.9933

Inversion and Wavelet Scaling

With these parameters, the inversion was then run on the full 3D data set. The first automated step in the inversion algorithm is scaling of the wavelet. In order to scale the impedances correctly in Equation-7, the absolute amplitude of the wavelet must be known. The wavelet shape has already been established, however the absolute amplitude has not. To solve for the wavelet amplitude, the unscaled wavelet **w** is convolved with the reflectivity of the initial guess model (**r**) and then correlated with $\mathbf{w}^T$ to give: $\mathbf{w}^T\mathbf{wr}$ (HRS Strata Theory). The RMS value of the ten largest amplitude peaks and troughs from this series is found

$$avgModelAmp = \sqrt{\left(\frac{1}{10}\right)\sum_{i=1}^{10}(w^T wr)_i^{\,2}}$$

Also, $\mathbf{w}^T\mathbf{T}$ is calculated (where **T** is the seismic trace) and the RMS value of the ten largest amplitude peaks and troughs of this series is found:

$$RMS\_TraceSize = \sqrt{\left(\frac{1}{10}\right)\sum_{i=1}^{10}(w^T T)_i^{\,2}}$$

The ratio:

$$\frac{avgModelAmp}{RMS\_TraceSize}$$

is used to scale the wavelet.

A key parameter used in scaling the wavelet is which seismic trace(s) **T** to use in the scaling algorithm. Because the seismic trace amplitudes were not equalized during the processing flow, the wavelet amplitude may not be consistent throughout the seismic data volume. This is illustrated FIG. 13 which shows the RMS of the seismic trace amplitude in a window from 150 ms above to 500 ms below the Upper Ardley Coal horizon. Over a window of this size, the RMS values should be fairly uniform, but they are not. Therefore, the inversion algorithm was parameterized to scale the wavelet for each trace individually.

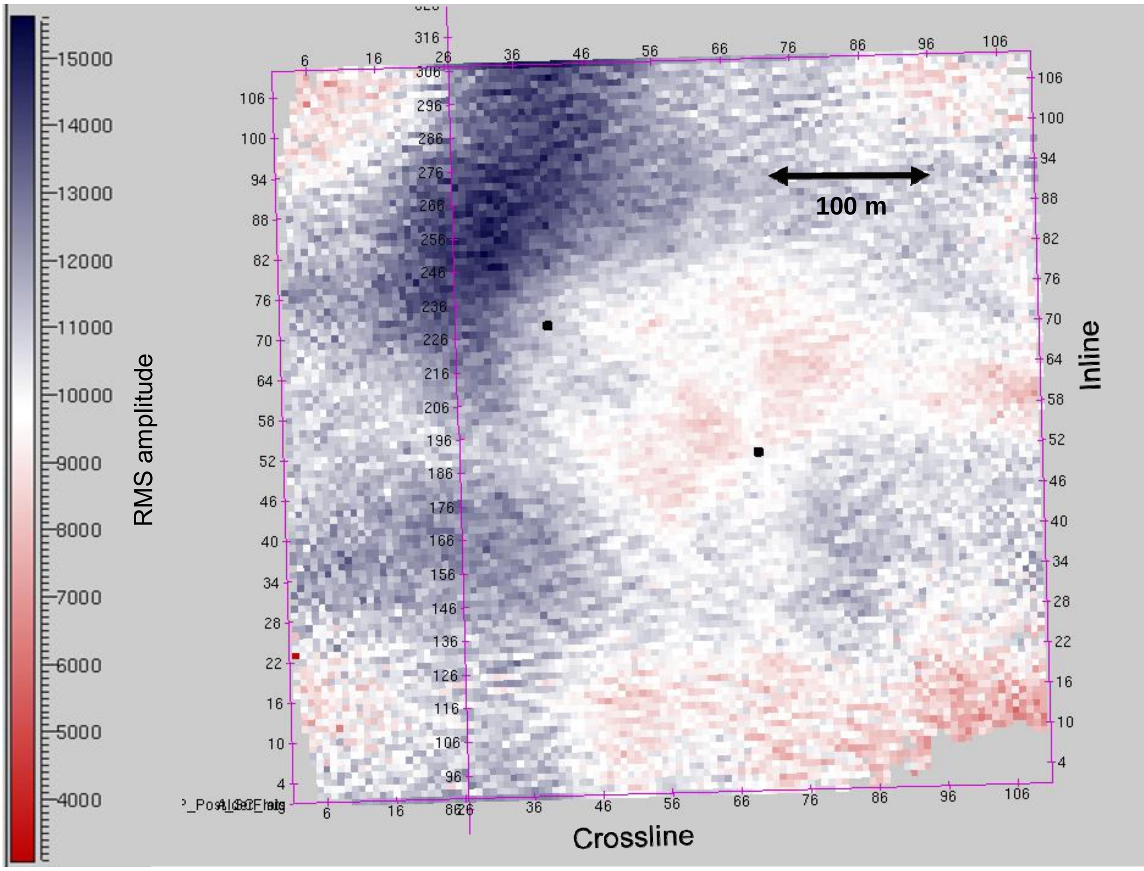

FIG. 13. The RMS of the trace amplitudes in the 3D data in a window from 150 ms above the Upper Ardley Coal horizon to 500 ms below the Upper Ardley Coal horizon.

The results after inversion are illustrated in FIG. 14. The figure can be compared to the low frequency initial guess model in FIG. 11. Two layers of low impedance occur after 300 ms which are the Lower and Upper Ardley Coals.

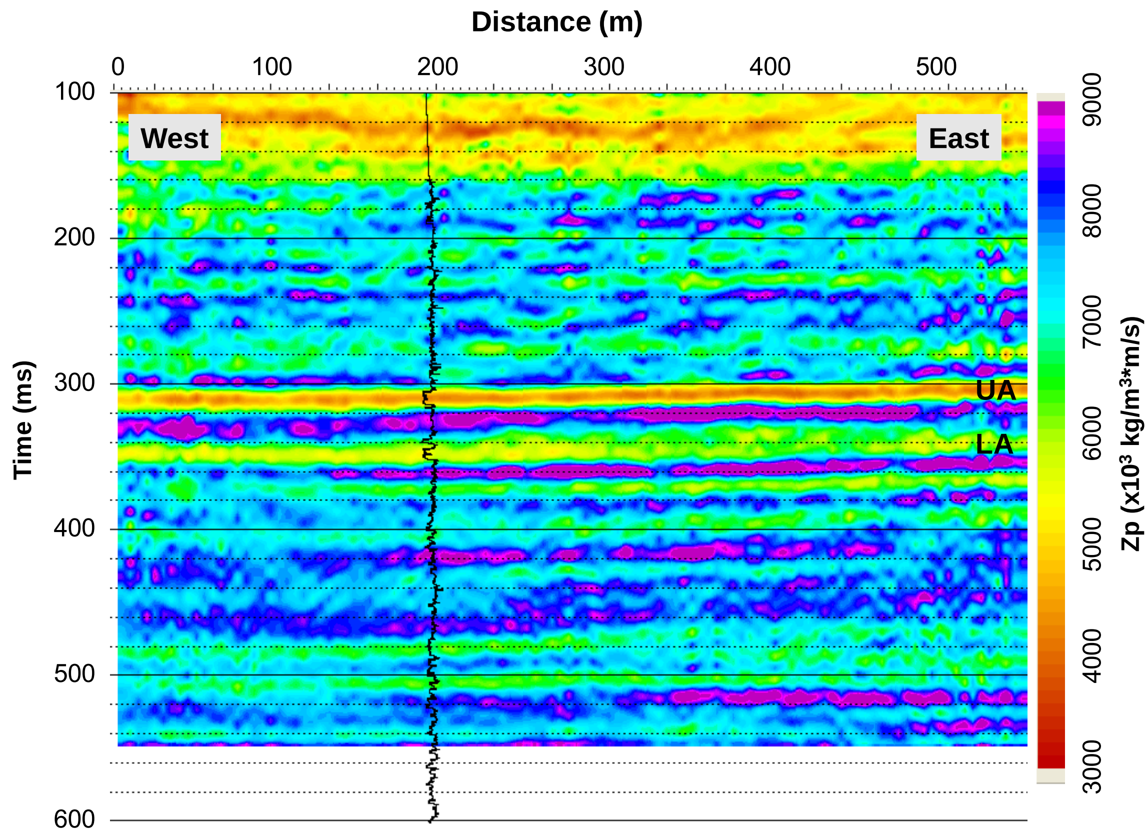

FIG. 14. The inverted impedance (inline 71) with the impedance log from 102/7-28 superimposed.

Interpretation

A closer inspection of the inversion of the Ardley Coal zone is illustrated in FIG. 15. Several trends are noteworthy. The Upper Ardley Coals are represented by a strong zone of low impedance that ties acceptably in time with the well impedance log. The event is laterally continuous and of uniform thickness, as intuitively expected. However, the Lower Ardley Coal impedance event does not show consistency or constant thickness. At the south end of the survey, the zone of low impedance is very much smeared out and using a lithology cut-off value of $6.0x10^6$ kg/m^3*m/s the coal zone effectively disappears. This phenomena can be related to the erratic character of the seismic trace at the Lower Ardley horizon in the south end of the survey which may be a related to the geology or it may be simply an unexplained data error (McCrank, MSc thesis in progress, expected 2008). However, in the vicinity of the 102/7-28 well, the inversion seems intuitively robust. The Mynheer and the Silkstone zones are not resolved as individual low impedance zones, but this is expected given the band-limited nature of the wavelet and the inversion.

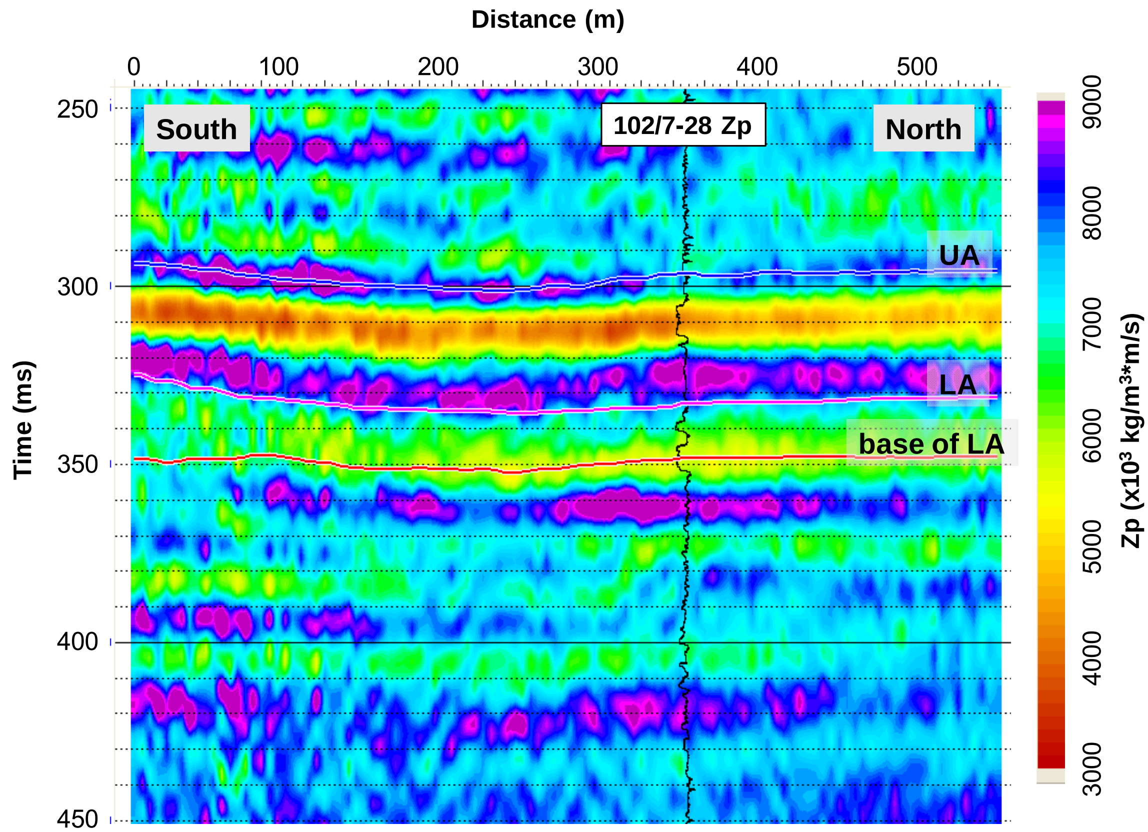

FIG. 15. The inverted impedance (cross-line 40) with the impedance log from 102/7-28 superimposed. The horizons are those picked from the seismic.

FIG. 15 shows that there is a low impedance zone in the Lower Ardley coals starting near the 102/7-28 well location. This anomaly is mapped in FIG. 16 which shows the average impedance in a window 2 – 12 ms above the "base of Lower Ardley" seismic horizon (FIG. 15). The map shows a distinct low impedance anomaly immediately to the northeast of the 102/7-28 well. The anomaly covers an elliptical area with major and minor axis lengths of approximately 65 m x 25 m (an area equivalent to 1276 m^2).

The size of the anomaly and its location suggest that it could be a related to the injected CO_2. The Alder Flats project engineers noted that if the CO_2 entered the full thickness of the Lower Ardley coal zone, the area of the region contacted by CO_2 would be 1,495 m^2 and that if the region were circular around the injection well (102/7-28) the equivalent radius would be 21.8 m (Mavor and Faltinson, 2008). Also, because the dominant natural fracture direction and the anticipated orientation of the hydraulically stimulated fracture trends southwest-to-northeast, the preferential permeability pathway is expected to be southwest-northeast and any injected fluid would move along that axis. Thus, the anomaly's location, shape and size suggest that it could be related to the injected CO_2.

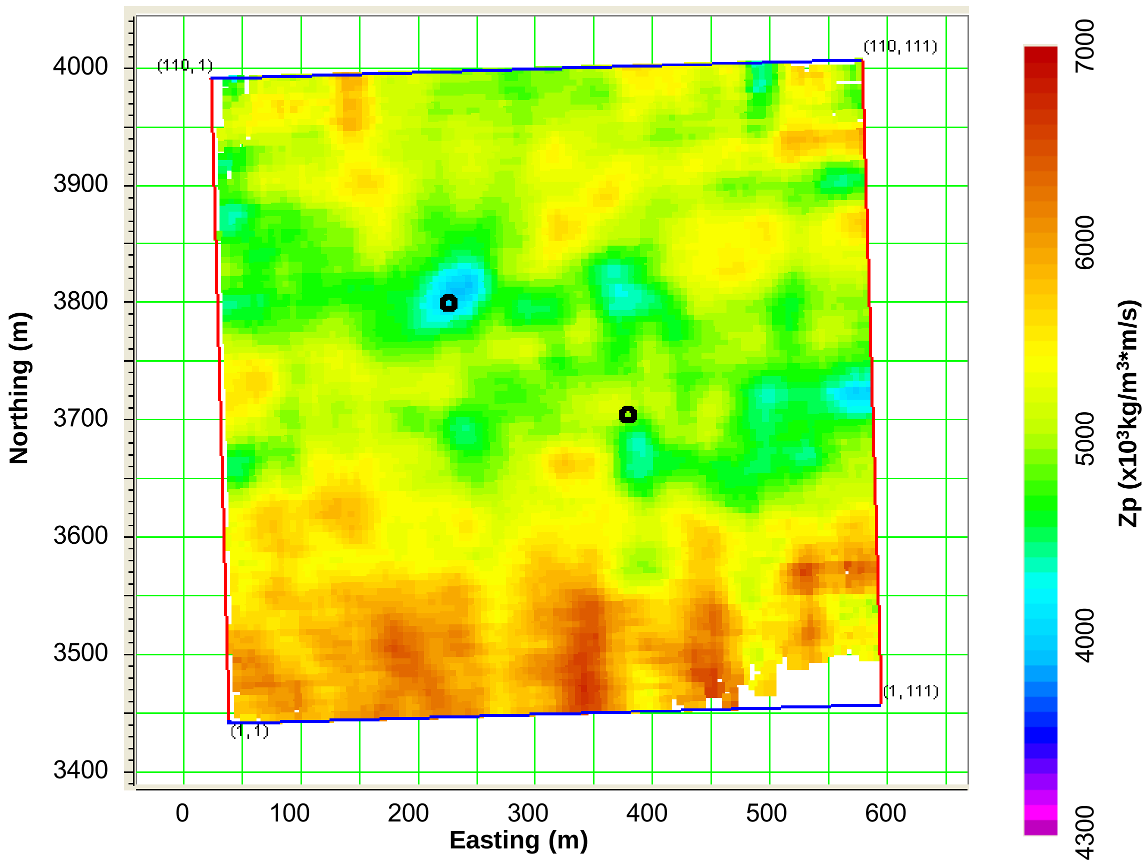

FIG. 16. A map of the mean impedance in a 10 ms window through the Lower Ardley impedance zone.

One method to QC (quality control) an inversion result is to look at the residual difference between seismic data and the synthetic seismogram that is created from the inverted impedance estimation. FIG. 17 illustrates the residual difference which is low throughout the data volume.

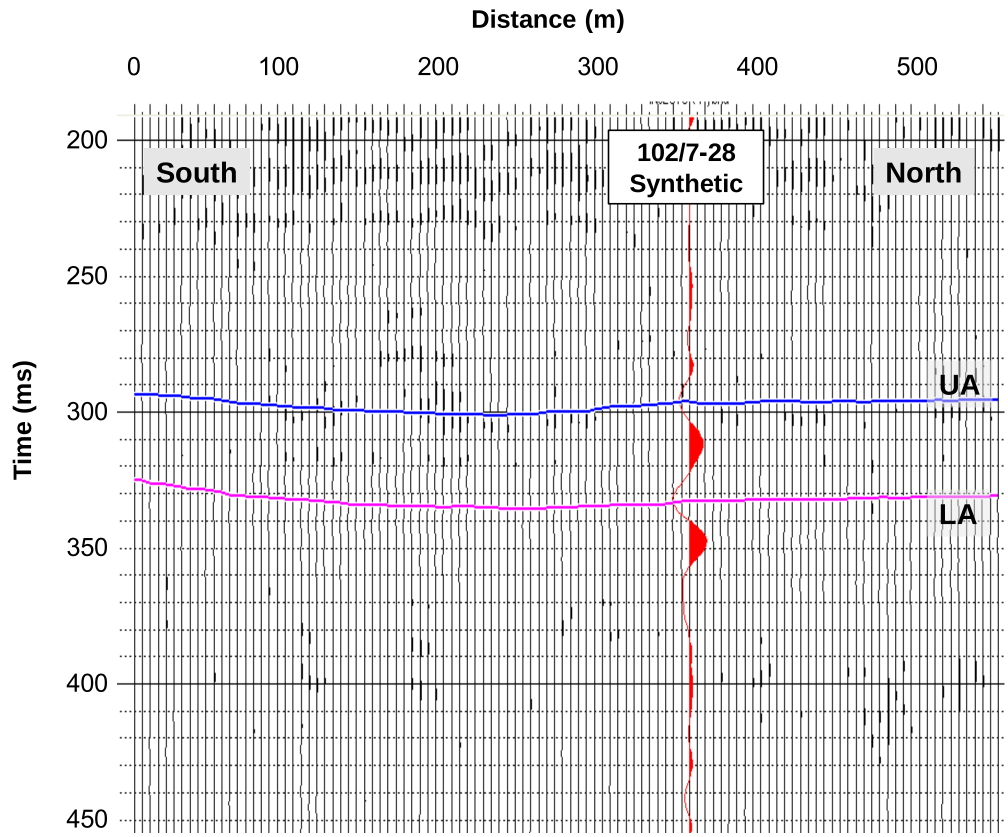

FIG. 17. The residual difference between the seismic traces and the synthetic seismogram created from the impedance estimation (cross-line 40).

Another method of QC'ing the inversion is to compare the impedance estimate to the known impedance at well locations. However, since the impedance estimate is band-limited, it is important to compare the inversion result to a band-limited version of the well log. FIG. 18 shows the comparison of the inverted impedance and the well log impedance from 102/7-28 well after high cut filtering (60-70 Hz). Generally the values of the inversion estimate are scaled comparably to the well log impedance. A cross-plot of the inversion impedance values and the filtered log values shows a 1:1 slope which confirms that the inversion scaling is unbiased (FIG. 19).

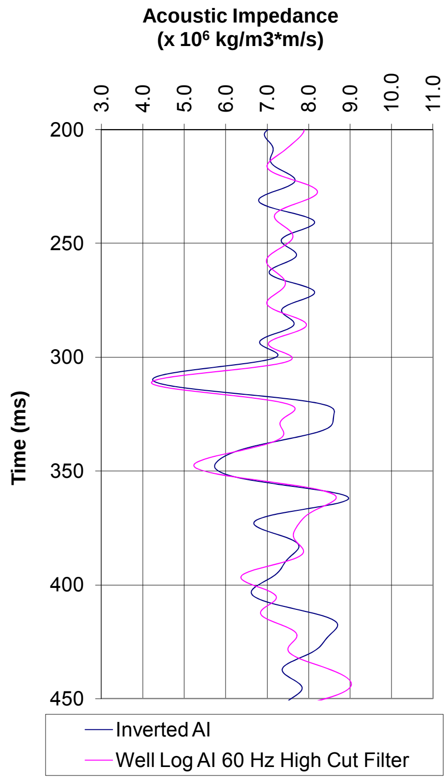

FIG. 18. The inverted impedance estimate and the 102/7-28 well log impedance after applying a 60-70 Hz high cut filter.

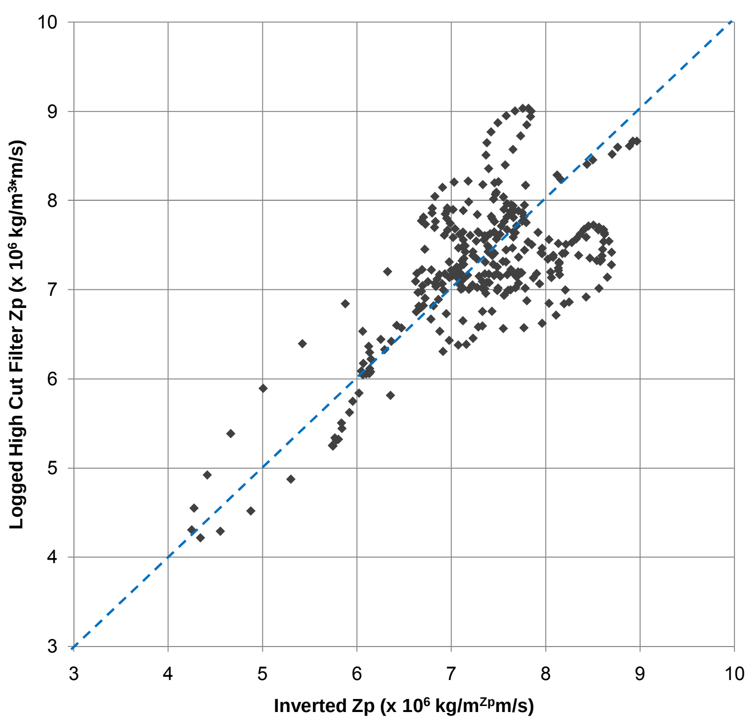

FIG. 19. Cross plot of the impedance inversion estimate values and the well log impedance values after high cut filtering (60-70 Hz).

(Author's note: HRS Strata includes a tool for doing a sparse spike inversion, as well as other inversion algorithms. However, only the model-based tool was used as a part of this work).

MIXED-NORM CONSTRAINED SPARSE SPIKE INVERSION OF THE ALDER FLATS 3D DATA

In order to verify the inversion results, the inversion was run with a different algorithm. The Jason Geoscience Workbench (JGW) uses a mixed-norm inversion algorithm called a Constrained Sparse Spike Inversion (CSS inversion). The CSS inversion was used to invert the Alder Flats data. The workflow for inversion with JGW is:

1. Estimate the wavelet shape and amplitude using the CSS inversion algorithm in reverse.
2. Build a low frequency trend model by interpolating well data throughout the model domain following specified seismic markers.
3. Test the λ norm-weighting parameter.
4. Identify the inversion constraints.
5. Run the inversion.
6. QC the results:
   - compare the residual difference between the seismic trace and the synthetic that would be created with the inverted impedance mode,
   - compare the amplitude of the inverted impedance to the well logs.

Wavelet Estimation

The JGW uses another technique to estimate the wavelet in the seismic data. The tool finds the wavelet that will best produce the log reflectivity from the seismic data using the CSS inversion. The 128 ms estimated wavelet extracted from 150 – 400 ms (where the well data is accurate) is illustrated in FIG. 20. The algorithm can optionally use a Papoulis taper that is harsher (tapers faster) than a cosine taper. The amplitude spectrum is only subtly different than the wavelet used in the model-based inversion.

A QC of the wavelet is to compare the amplitude spectrum of the wavelet in the Fourier domain to the spectrum of the seismic data. The wavelet's spectrum should not be too dissimilar to the seismic data spectrum for a white Earth but should be shifted with respect to that for the seismic for a coloured Earth. FIG. 21 illustrates the comparison and shows that the wavelet spectrum is roughly a smoothed version of the seismic spectrum. The seismic spectrum has more peaks and troughs but this is expected since the reflectivity series spectrum also shows many peaks and troughs (FIG. 22). Windowing and tapering the wavelet in the time domain smoothes the wavelet spectrum in the Fourier domain, so the window length and taper must be selected carefully. FIG. 21 shows that the wavelet spectrum does represent a smoothed (shifted) version of the band-limited reflectivity series and thus appears to be accurately parameterized.

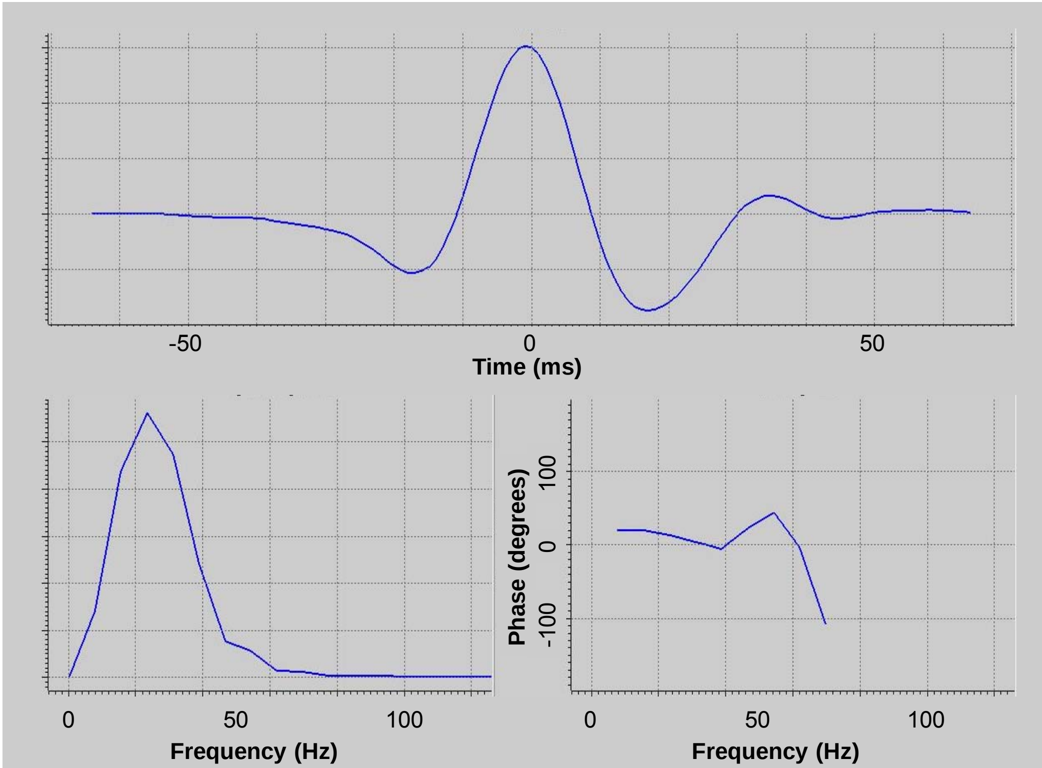

FIG. 20. The wavelet estimated using the CSS inversion.

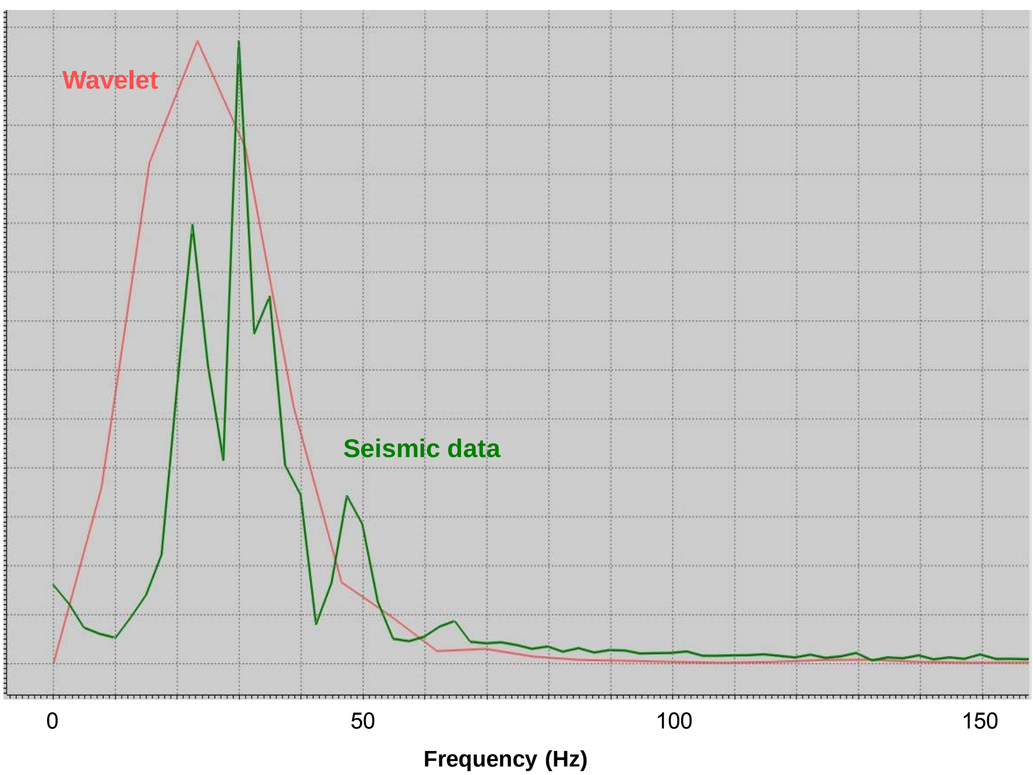

FIG. 21. The amplitude spectrum of the wavelet and the seismic data.

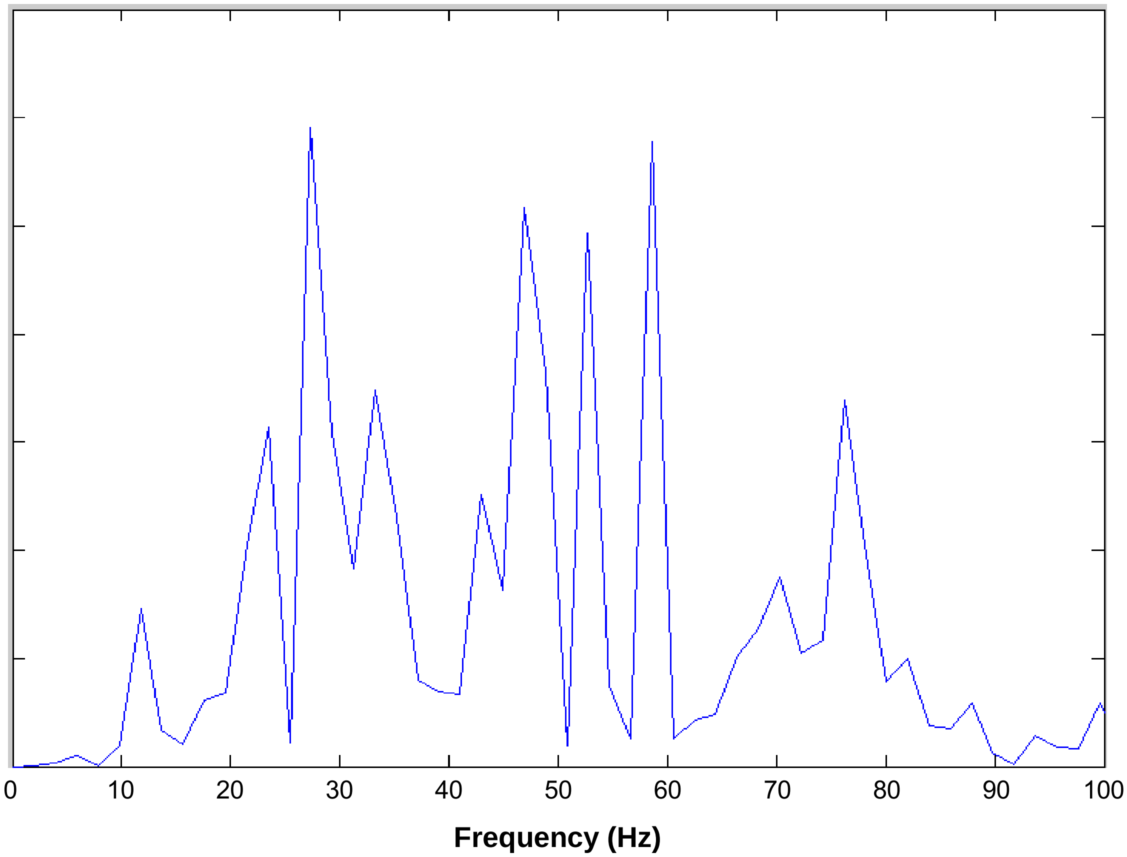

FIG. 22. The amplitude spectrum of the reflectivity series from the 102/7-28 well logs generated from a 512 ms time series with 1 ms sampling and an 80-120 Hz high-cut filter.

Although the CSS inversion can accommodate a spatially varying wavelet, it is convenient to assume that there is a single wavelet with a constant amplitude throughout the seismic volume. For this to be valid, it is important that the amplitudes of the seismic data are balanced from trace to trace. As discussed above, the data showed a significant variation in RMS amplitude in a long time window around the Ardley Coal reflection events which indicated that the trace amplitudes were not equally balanced. Therefore the RMS amplitudes were normalized over this 650 ms window before proceeding with the inversion.

Setting the Inversion Parameters

The CSS inversion minimizes a mixed norm objective function:

$$J = L_p(\mathbf{r}) + \lambda L_q(\mathbf{T} - \mathbf{wr}) + L_1(\text{low freq. residuals})$$

where λ weighs between the first term that seeks the sparsest reflectivity series possible, while the second term seeks to minimize the difference between the seismic trace and the model trace (wavelet convolved with the solution reflectivity series) in a least squares sense. The choice of λ depends upon the level of noise in the seismic data and is a critical parameter to adjust. If λ is too small, the reflectivity will be sparse, but the model will not closely match the seismic. However, if λ is too large, the model will match the trace very well, but there will be too many reflection coefficients in the solution series, some of which will merely model the noise. The key is to find the λ value that just matches the seismic. FIG. 23 shows two methods of evaluating the correct choice of λ. FIG. 23a shows the seismic trace and the residual between the model trace and the seismic at the same amplitude scale. Setting λ to 10 appears to be the lowest level that produces a small residual. FIG. 23b shows the resulting impedance inversion for several traces and compares it to the well log impedance values. Again a λ value of 10 produces an adequate match between the inversion impedance and the well log impedance.   was set to 10 in the inversion.

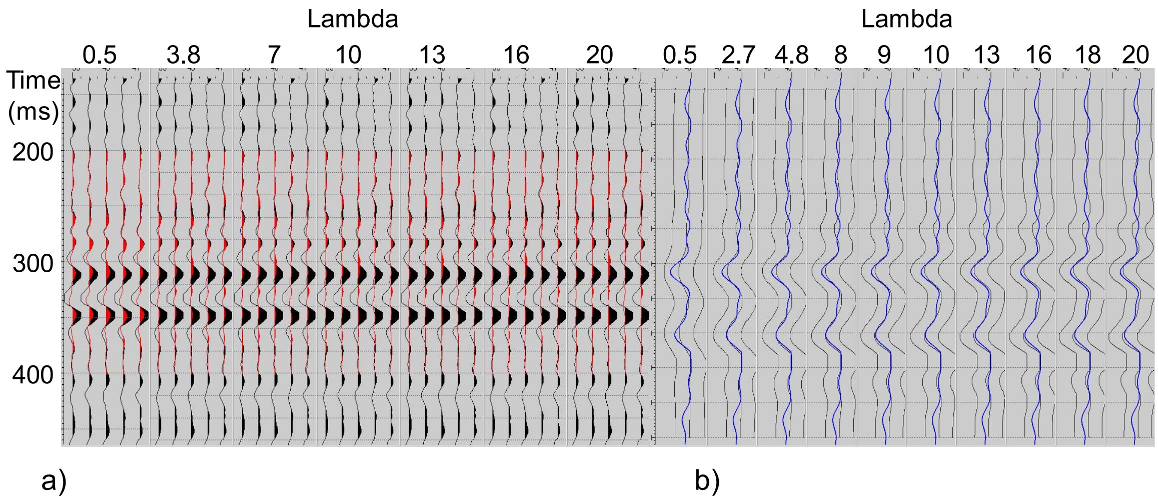

FIG. 23. Testing the λ value. (a) the seismic and the residual in the time domain and (b) the inverted impedance (black) compared to the well log impedance (blue).

The third term in the objective function softly constrains the low frequencies in the inversion to match the low frequencies in the model. The CSS inversion objective function also includes an optional constraint that constrains the solution to stay within a specified range of the solutions in adjacent CDP bins. This introduces stability in the inversion and results in a smoother inversion result bin-to-bin. The inversion was constrained in this way.

The solution to the inversion is a reflectivity series. The impedance is estimated using Equation-2 and constraints from the low frequency model. Finally, the estimated impedance is merged with the low frequency model to produce the inverted impedance. The frequency at which to merge the estimated impedance with the low frequency model must be specified. The low frequency model used in the CSS inversion was essentially identical to the model illustrated in FIG. 11 which was filtered with a 10-15 Hz filter. This was an appropriate merging band since the source vibroseis sweep started at 10 Hz.

Inversion QCs

FIG. 24 shows the inverted impedance and the band-limited impedance well log from 102/7-28. As before, in the cross-line direction (north-south) the impedance in the Upper Ardley coal zone is consistent across the survey, but in the Lower Ardley coal zone the impedance estimate shows the same deterioration in consistency seen in the model-based inverted impedance at the south end of the survey. The inverted impedance estimate is illustrated alongside the original seismic data in FIG. 25. FIG. 25 also shows that the horizons for the Lower and Upper Ardley coal zones can be picked either on the seismic troughs or on the impedance data using a 6.0×10^6 kg/m^3*m/s cut-off.

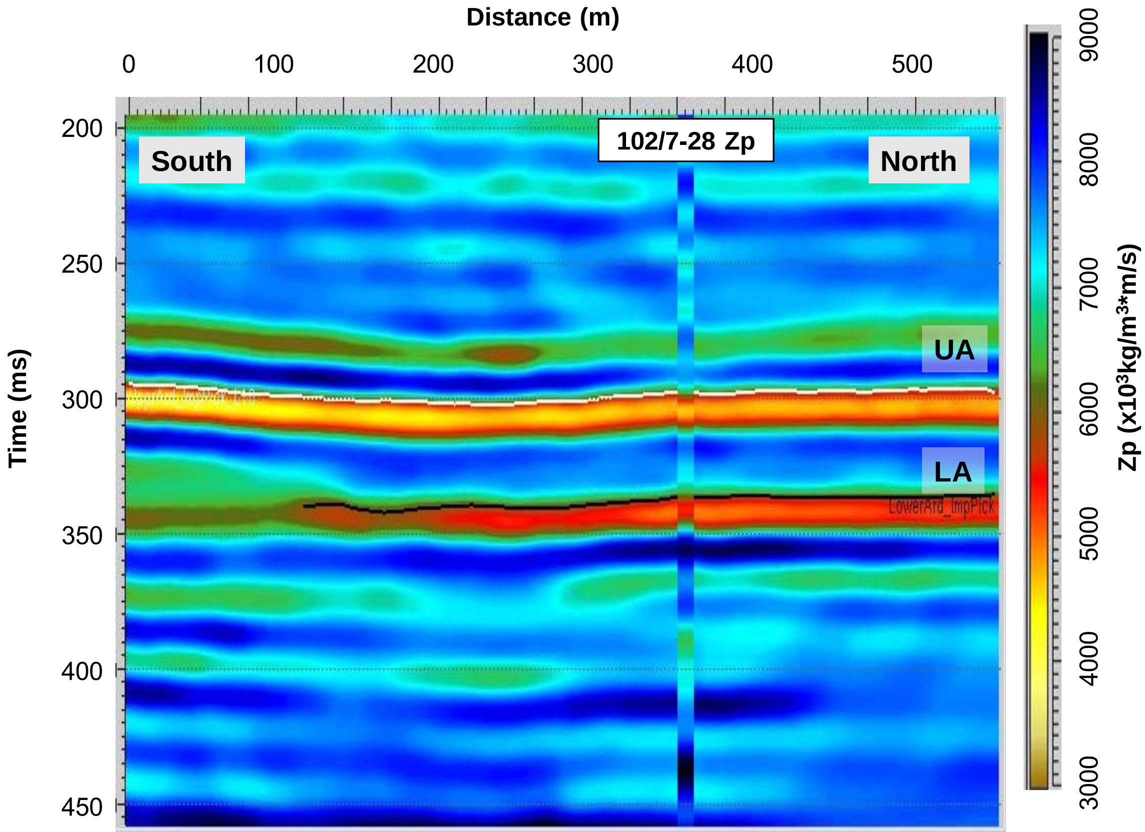

FIG. 24. The inverted impedance (cross-line 40).

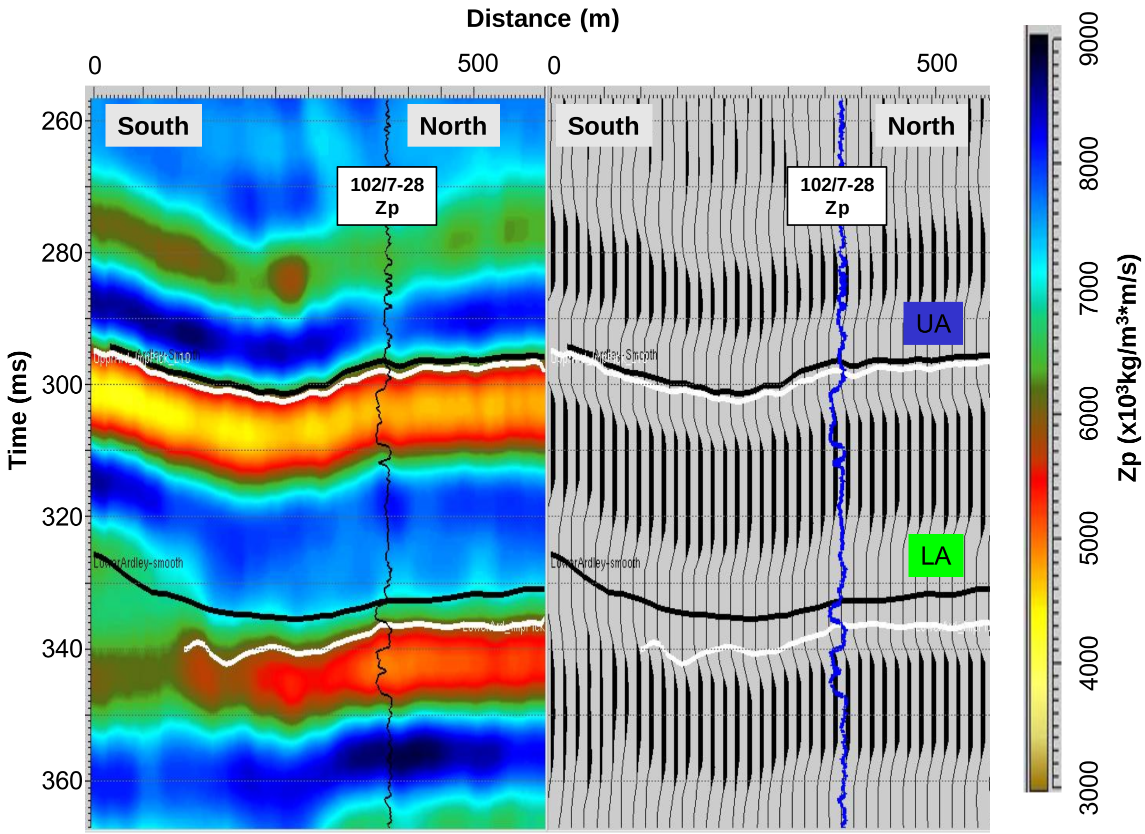

FIG. 25. The inverted impedance (cross-line 40) and the original seismic. Lower and Upper Ardley coal horizon picked on seismic (black) and on the impedance data $6.0x10^6$ $kg/m^3*m/s$ cut-off (blue).

The cross-correlation between the synthetic seismograms generated from the inverted impedance and the original seismic traces over a 200 ms window around the Ardley coals (FIG. 26) is higher than 0.9 throughout most of the survey indicating a good match. FIG. 27 shows the residual difference between the original seismic data and the seismogram generated from the inversion impedance with the original seismic superimposed (each at the same scale). The residual is low relative to the seismic especially in the window of the Ardley coals.

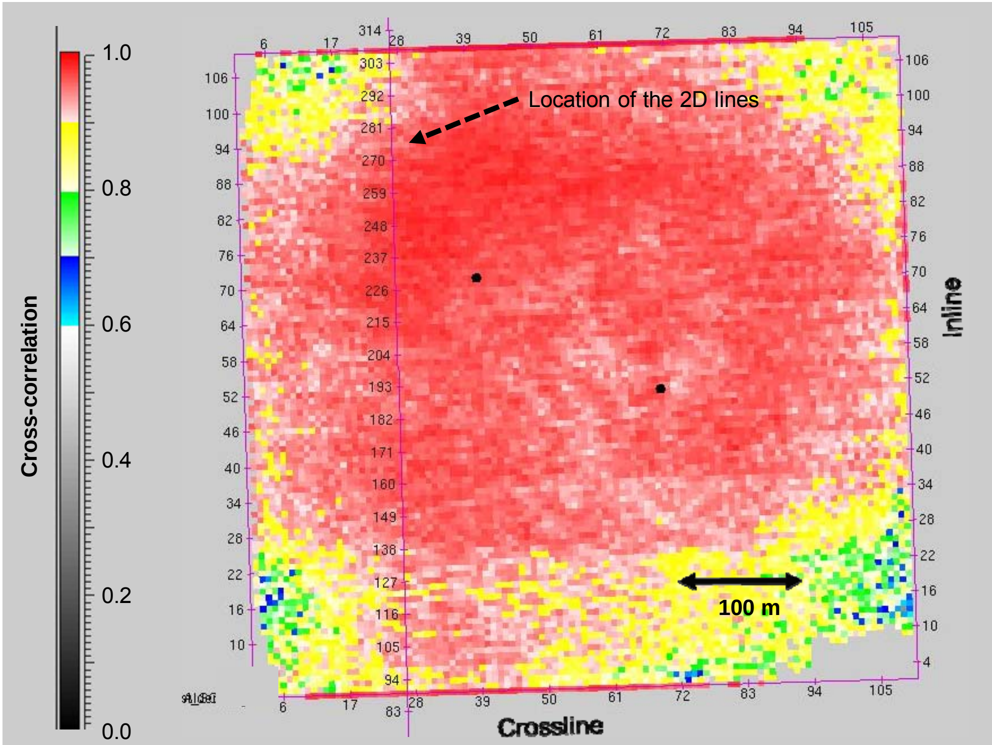

FIG. 26. Inverted synthetic seismogram cross-correlation with the seismic data.

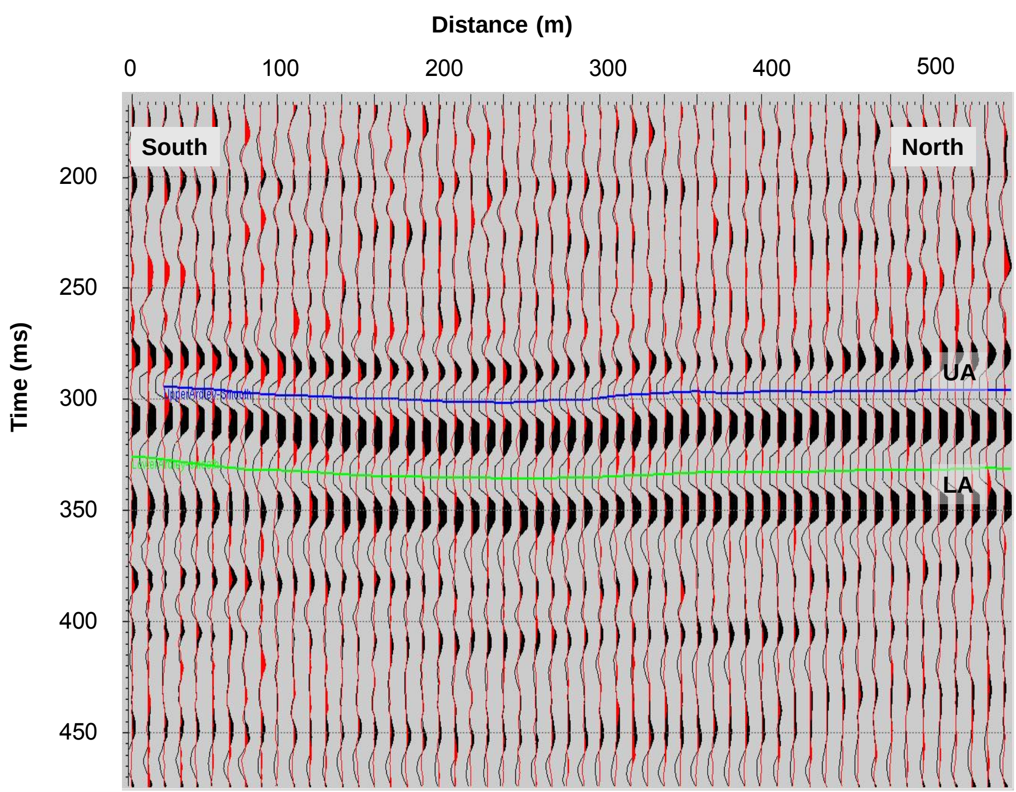

FIG. 27. The seismic data (black) and the residual error (red) plotted at the same amplitude scale (cross-line 40).

The scale of the inverted impedance is compared to a band-limited version of the well log impedance in FIG. 28 which shows that the inverted impedance is a slightly higher in the Upper Ardley coal zone and is slightly lower in the Lower Ardley coal zone than the high cut filtered well log impedance. However, overall, the amplitude is approximately correct. FIG. 29 shows the cross-plot of the inverted impedance estimates to the band-limited well log impedance values. The trend shows a 1:1 slope indicating an unbiased and generally correctly scaled impedance estimate.

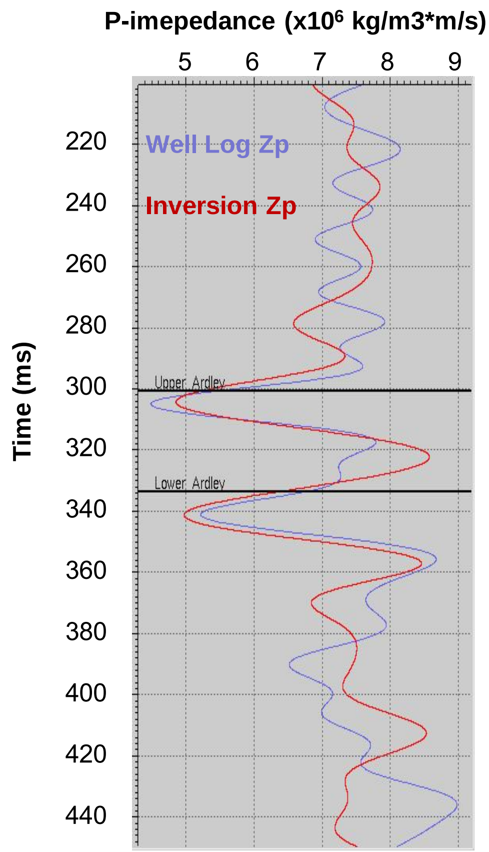

FIG. 28. The inverted impedance and the 102/7-28 well log impedance with a 60-70 Hz high cut filter.

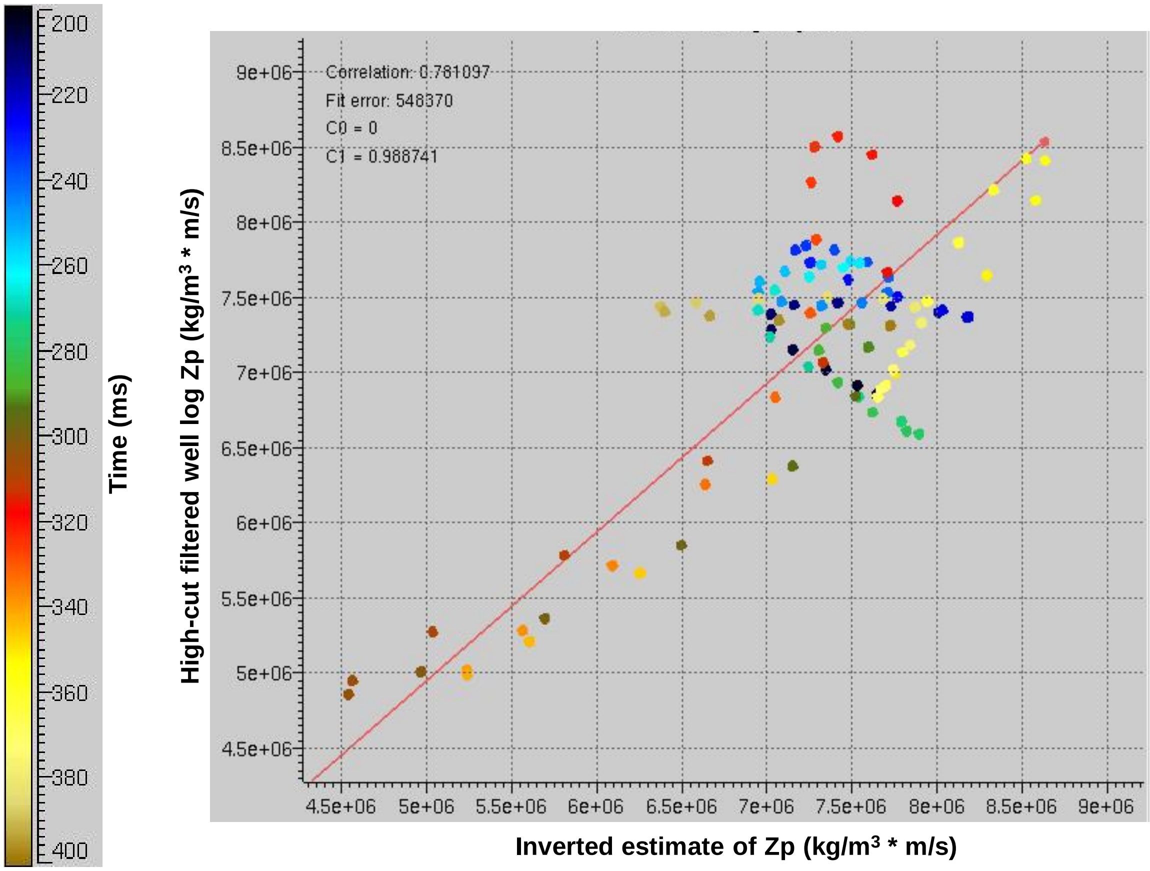

FIG. 29. The cross-plot of the inverted impedance and the well log impedance after high cut filtering (60-70 Hz).

Interpretation

FIG. 30 shows a close scrutiny of the inversion results. In FIG. 30a, the impedance well log with a 60-70 Hz high cut filter is superimposed on the inverted impedance result. A slight time delay in the impedance estimate of the Lower Ardley coal is evident which could be a residual effect of a phase delay in the Lower Ardley seismic event resulting from short-path multiples (see McCrank, MSc Thesis, in progress 2008). FIG. 30c shows the reflectivity result of the CSS inversion. It is interesting to note that although the Mynheer and Silkstone coals zones were not resolved as separate events in the seismic data or the impedance estimate, there is a subtle event in the estimated sparse spike reflectivity series (FIG. 30c) that could be tied to the thin zone of the Silkstone coal zone.

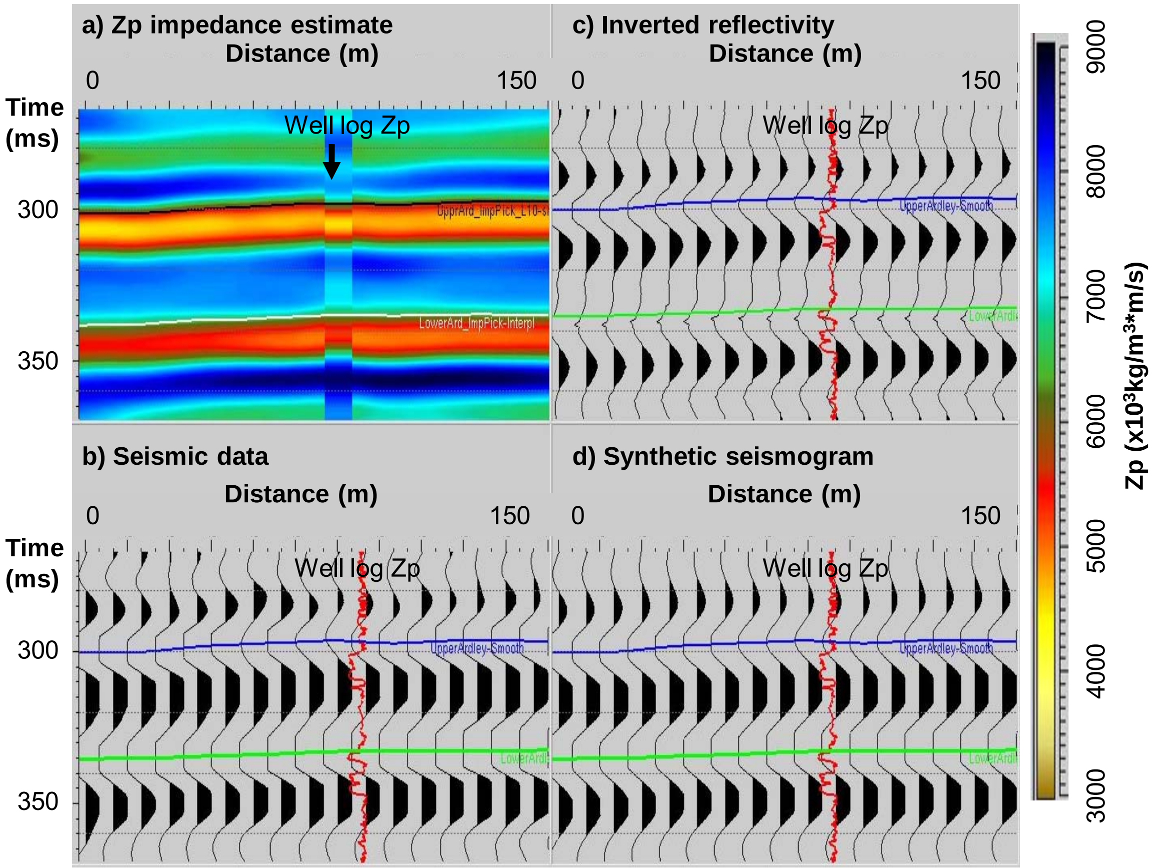

FIG. 30. (a) The inverted impedance with the well log impedance after 60-70 Hz high cut filtering, (b) the original seismic, (c) the inverted reflectivity, and (d) the inverted synthetic seismogram (a portion of cross-line 40).

Horizon slices at 1 ms increments to the Lower Ardley coal zone seismic horizon are mapped in FIG. 31. The slices effectively step through the impedance of the Lower Ardley coal zone. At a horizon that is 10 ms below the Lower Ardley horizon a low impedance anomaly is evident around the 102/7-28 well. FIG. 32 illustrates this slice again and the temporal location of the slice. An anomaly is evident again to the northeast of the well in exactly the same location that it was observed in FIG. 16. Its approximate areal extent is 1800 m^2.

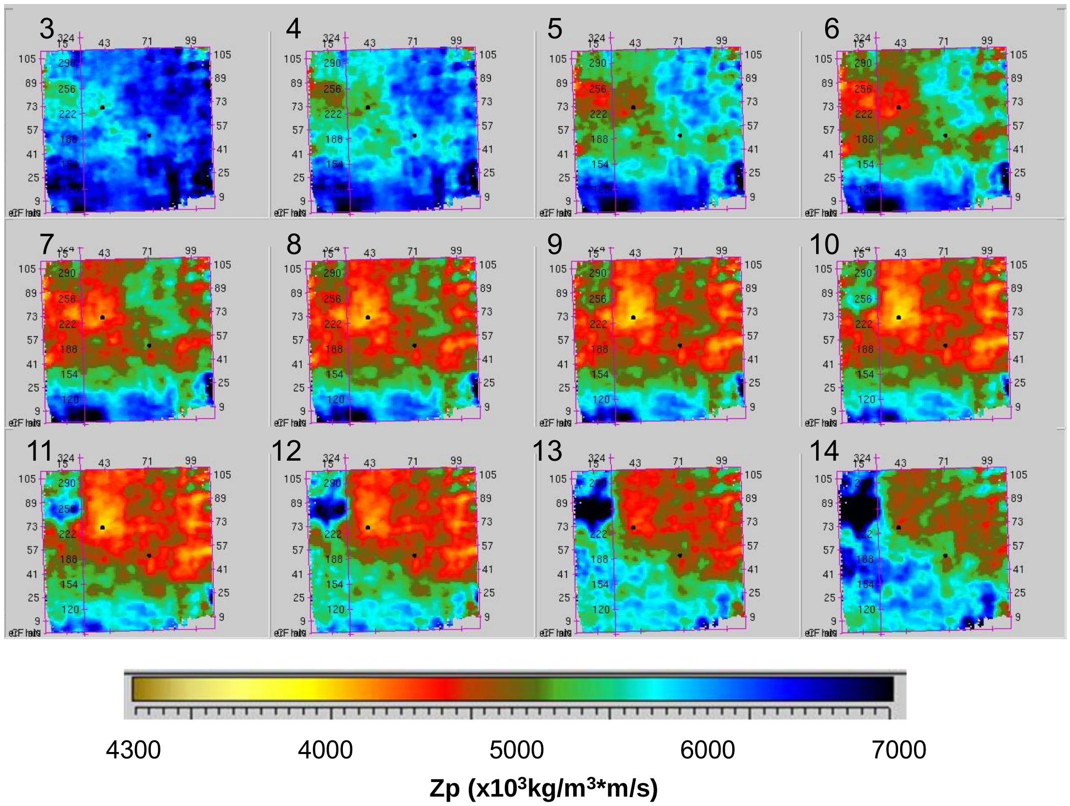

FIG. 31. 1 ms steps through the inverted impedance of the Lower Ardley coal zone from 3 - 14 ms below the Lower Ardley coal seismic pick horizon.

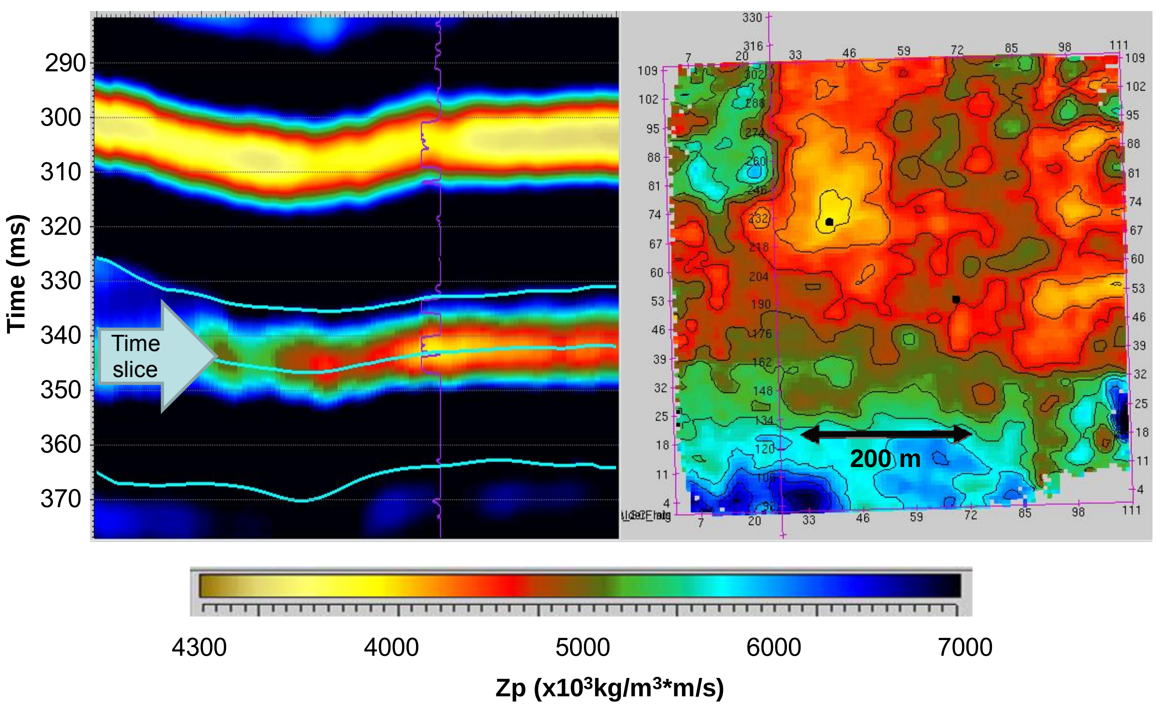

FIG. 32. Examination of a horizon slice through the middle of the Lower Ardley coal low impedance zone and cross-line 40 showing the slice location.

The mean impedance in a 10 ms window below the Lower Ardley coal horizon picked from the impedance volume (using the $6.0\text{x}10^6$ kg/m^3*m/s cut-off) is illustrated in FIG. 33. Again the anomaly is evident. FIG. 34 illustrates a 3D rendering of all impedance samples that are less than $5.0\text{x}10^6$ kg/m^3*m/s and that are connected to at least 49 other similar samples (i.e. clusters of 50 or more connected impedance voxels less than $5.0\text{x}10^6$ kg/m^3*m/s). The sheet of the Upper Ardley coal zone is obvious at the top of the volume where the thickness of the coal zone has resulted in this very low impedance estimate. The figure also shows the extent of the very low impedance anomaly cluster in the Lower Ardley coal zone.

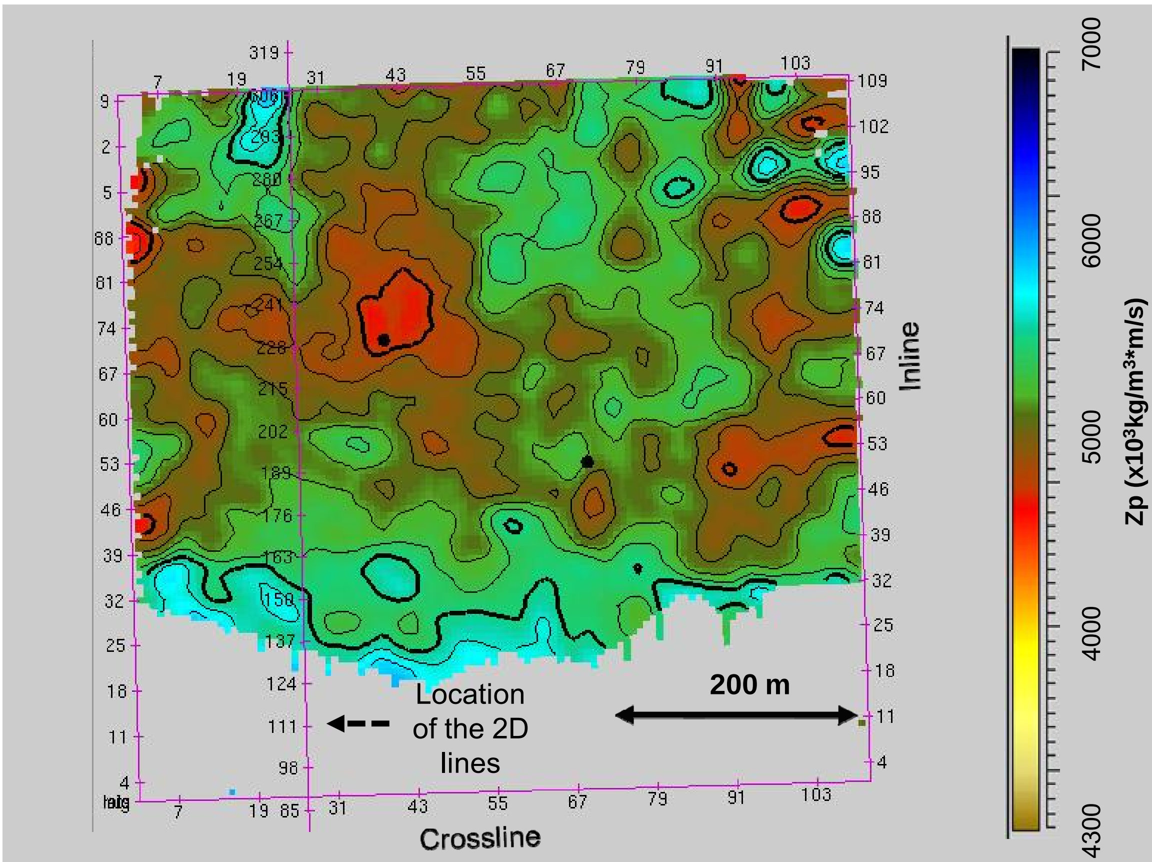

FIG. 33. The mean impedance in a 10 ms window below the Lower Ardley horizon picked from the impedance volume. Note the location of the 2D lines relative to the low impedance anomaly.

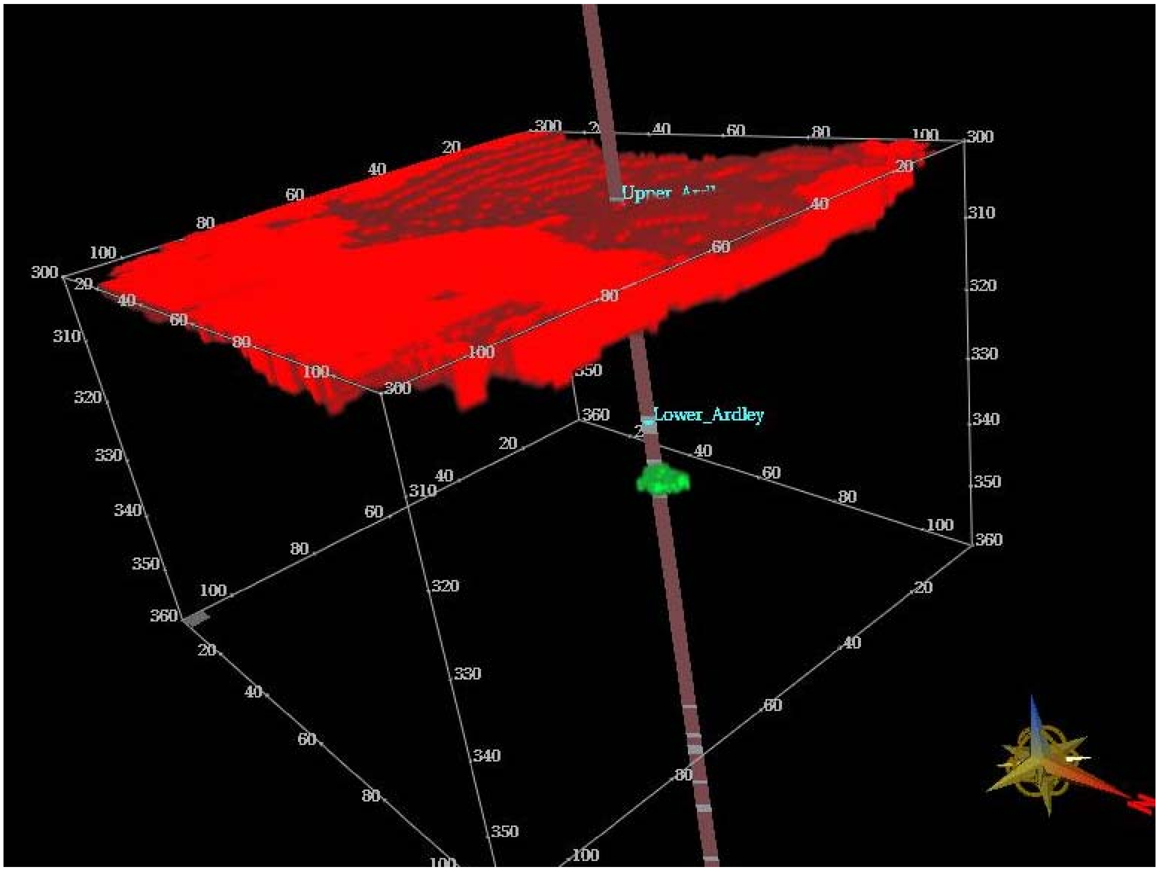

FIG. 34. 3D rendering of the clusters of area where the impedance is less than 5.0×10^6 kg/m^3*m/s. Note the Upper Ardley coal forms the large cluster in red, while a sole cluster exists in the Lower Ardley coal zone (green).

PETROPHYSICAL INTERPRETATION OF THE ANOMALY

Both the model-based and CSS inversion results show a low impedance anomaly around the 102/7-28 well in the Lower Ardley coal zone. The size, shape, and location of the anomaly correspond to the expected imprint of the 180 tonne CO_2 flood.

FIG. 32 illustrates that the impedance measured in the Lower Ardley coal anomaly reaches low values that are less than 5.0×10^6 kg/m^3*m/s while the rest of the Lower Ardley coal zone the impedance estimate is in the range of 5-6x10^6 kg/m^3*m/s. FIG. 8 showed a band-limited version of the impedance log from the 102/7-28 well and demonstrated that the minimum impedance in the 102/7-28 well was greater than 5.0×10^6 kg/m^3*m/s after high cut filtering. This discrepancy between the well logged impedance estimate and the impedance estimate from inversion in the Lower Ardley coal zone suggests that the impedance may have been lowered in the vicinity of the 102/7-28 well after the logging data was acquired.

FIG. 35 shows the 102/7-28 impedance well log at “logging resolution” and at “seismic resolution” (after application of a 60-70 Hz high cut filter). The band-limited impedance log is higher than 5.0×10^6 kg/m^3*m/s. Also shown is a log where the impedance of the Mynheer coal zone has been lowered uniformly by 10%. The reduced impedance log after application of the high cut filter is also shown. It indicates that a 10%

reduction in the impedance of the Mynheer coals would be enough to change the band-limited impedance estimate to just less than 5.0x10^6 kg/m^3*m/s.

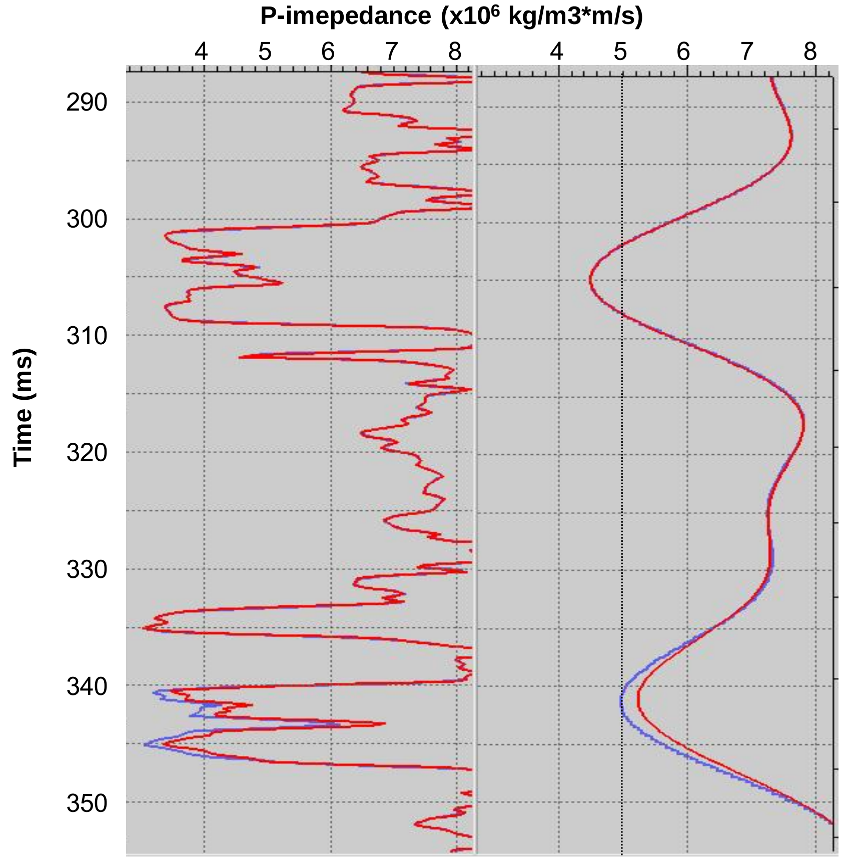

FIG. 35. The original impedance log from the 102/7-28 well (red) and the log adjusted by a 10% reduction in impedance in the Mynheer coal zone (blue). The curves are at log resolution on the left and with a 60-70 Hz high cut filter on the right.

It is reasonable to ask whether a fluid substitution of water for gaseous CO_2 in the coals' macroporosity cleat system could account for the level of anomaly observed in the measured impedance of the Lower Ardley coals if calculated with the Gassmann model.

The Gassmann fluid substitution model assumes that fluid substitution occurs only in the macro-porosity of the coal. The Mynheer coals in their original state were likely water saturated and the logged data was used to find the water saturated elastic properties. The average velocity and density values from the logs were used to find the average values for the water saturated rock listed in Table 3. The shear modulus of the rock was assumed to be unchanged by a substitution of fluids, and so the dry shear modulus and the shear modulus when the coal macro-porosity was filled with CO_2 is the same as the shear modulus measured with the petrophysical logs. The bulk modulus and density of water and CO_2 were calculated using methods described by Batzle and Wang (1992). The fracture porosity was assumed to be 1%, as indicated by Mavor and Faltinson (2008).

Estimating a bulk modulus for the dry rock frame (K_{fr}) is difficult. Ideally, lab measurements of the dried frame would be available. Alternatively, literature values could be used. However, neither of these was available. Castagna et al. (1993) showed that the Vp/Vs ratio was the same for wet and dry coals, although the authors conceded that the conclusions were based on a limited data set and the there was no consideration for the effect of coal sub-lithology on the relationship. For lack of a better estimate, it was assumed that the bulk modulus of the dry coal frame is 10% less than the water saturated bulk modulus. Given the low fracture porosity this is an appropriate estimate.

The Gassmann equation is:

$$\frac{K_{sat}}{K_0 - K_{sat}} = \frac{K_{fr}}{K_0 - K_{fr}} + \frac{K_f}{\phi\left(K_0 - K_f\right)} \tag{8}$$

where ø is porosity, K_{sat} is the bulk modulus of the fluid saturated rock, K_{fr} is the bulk modulus of the dry rock frame, K_o is the bulk modulus of the rock mineral, and K_f is the bulk modulus of the fluid.

With ϕ, K_{sat}, K_{water}, and K_{fr} estimated, Equation-8 can be used to calculated the bulk modulus of the coal mineral, K_o. All these data are listed in Table 3. Equation-8 can be re-arranged to give Equation-9 which is used to find the bulk modulus of the CO_2 saturated coal.

$$K_{sat} = K_{fr} + \frac{(1 - \frac{K_{fr}}{K_o})^2}{\frac{\phi}{K_f} + \frac{(1-\phi)}{K_o} - \frac{K_{fr}}{K_o^2}} \tag{9}$$

Finally the density can be calculated using:

$$\rho = \phi\rho_f + (1-\phi)\rho_o \tag{10}$$

The velocity and density values of the fluid saturated coals give the impedance, which for the water saturated coals is $4.61\text{x}10^6$ kg/m^3*m/s and for the gaseous CO_2 saturated coals is $4.43\text{x}10^6$ kg/m^3*m/s. This corresponds to a 3.9 % decrease in impedance when water is displaced by CO_2 in coals.

Table 3. The average elastic properties of the Mynheer coals used to model the substitution of water for CO_2 using the Gassmann method.

ϕ (macro)	0.01
V_p (water saturated)	2567 m/s
V_s (water saturated)	1097 m/s
ρ_{sat} (water)	1797 kg
k_{sat} (water)	8.96 GPa
μ_{sat} (water) = μ_{dry} = μ_{sat} (CO_2)	2.16 GPa
k_{water} (16.6 °C, 1.73 MPa, 1931 ppm NaCl)	2.4 GPa
k_{CO_2} (16.6 °C, 1.73 MPa)	0.01 GPa
ρ_{water} (16.6 °C, 1.73 MPa, 1931 ppm NaCl)	1002 kg/m^3
ρ_{CO_2} (16.6 °C, 1.73 MPa)	0.050 kg/m^3
v_p (dry coal)	2480 m/s
ρ (dry coal)	1779 kg/m^3
k_{fr}	8.06 GPa
k_o	9.21 GPa
k_{sat} (CO_2)	8.08 GPa
ρ_{sat} (CO_2)	1788 kg/m^3
v_p (CO_2)	2476 m/seismic
p-impedance (water saturated)	4.61 x 10^6 kg/m^3*m/seismic
p-impedance (CO_2 saturated)	4.43 x 10^6 kg/m^3*m/seismic

DISCUSSION AND CONCLUSIONS

Although the 3.9% impedance change predicted with the Gassmann model is not enough to explain the apparent 10% or greater change in the impedance observed in the vicinity of the 102/7-28 well in the inversion result, it is the right order of magnitude and could be argued to be the cause of the impedance anomaly. However, it is not a unique interpretation. Two similar interpretations are that the anomaly could be related to methane in the cleat system or a mixture of methane and CO_2 in the cleat system that would have a similar effect on the impedance. Another possibility is that the CO_2 has dissolved into the coal matrix and, as described above, reduced the elastic moduli of the coal frame itself (although this interpretation is more speculative given the dearth of experimental data in this area).

Other geological models are also possible. It has been noted that the Mynheer coal zone is laterally very heterogeneous (Pana, 2007) and that different sub-lithologies of the coal zones have different impedance values. It is possible that the low impedance zone results from an area of greater net pure coal versus shaley coal or coaly shale, or that either of the Mynheer or Silkstone coal zones thickens to the northeast of the 102/7-28 well which causes the low impedance anomaly. Other explanations for the low impedance zone could include reduced rock competency due to fracture stimulation procedures, effects due to the injection of water during the stimulation procedure, effects related to changes in reservoir effective pressure, subtle tuning effects that are not resolved by the inversion despite an accurate estimation of the embedded wavelet, or even seismic acquisition footprint effects. Differentiating between these possibilities in a conclusive, deterministic manor is not possible with the given data. Ultimately the only way to conclusively attribute a seismic anomaly to a reservoir change with production activities is to acquire a baseline and monitor seismic survey and analyze the data using time-lapse methods.

However, despite the shortcomings of the available data, attributing the low impedance anomaly to effects due to CO_2 injection remains a realistic explanation that requires few contrived assumptions. Given its proximity to the well, its alignment with the known preferential permeability pathway, and its dimensions, interpreting the anomaly as a signature of the CO_2 is reasonable.

ACKNOWLEDGEMENTS

The authors would like to thank the sponsors of the CREWES project, the volunteers and workers who contributed to the field acquisition, and the dedicated staff and students of CREWES and the University of Calgary Geoscience Department for assistance, discussion and inspiration.

We would also like to thank Hampson Russell and Fugro-Jason for providing access to software, assistance and advice.

REFERENCES

Aster, R.C., Borchers, B., Thurber, C.H., 2005, Parameter estimation and inverse problems: Elsevier Academic Press.

Avseth, P., M. Tapan, Mavko, G., 2005, Quantitative seismic interpretation : applying rock physics tools to reduce interpretation risk, Cambridge University Press.

Batzle, M., Wang, Z., 1992, Seismic properties of pore fluids: Geophysics, **57**, no. 11, 1396-1408.

Castagna, J. P., Batzle, M.L., Kan, T.K., 1993, Rock Physics – The link between rock properties and AVO response, from: Offset-dependant reflectivity – theory and practice of AVO analysis, published by the Society of Exploration Geophysicists, edited by Castagna, J, and Backus, M..

Cooke, D., Schneider, W., 1983, Generalized inversion of reflection seismic data: Geophysics, **48**, n. 6, p. 665-676.

Day, S., Fry, R., Sakurovs, R., 2007, Swelling of Australian coals in supercritical CO_2: International Journal of Coal Geology, 12 pages.

Debeye, H.W.J., van Riel, P., 1990, L_p-norm deconvolution: Geophysical Prospecting, **38**, p. 381-403.

Gale, J., and P. Freund, 2001, Coal-bed methane enhancement with CO2 sequestration worldwide potential: Environmental Geosciences, **8**, p. 210–217.

Hampson Russell Strata Software Theory, online with Hamspon Russell Software.

Karacan, C.O., 2007, Swelling-induced volumetric strains internal to a stressed coal associated with CO2 sorption: International Journal of Coal Geology, **72**, 209-220.

Khan, M.R., Jenkins, R.G., 1985. Thermoplastic properties of coal at elevated pressures: effects of gas atmospheres. Proc. Int. Conf. On Coal Science, Sydney.

Larsen, J.W., 2004, The effects of dissolved CO_2 on coal structure and properties. International Journal of Coal Geology, **57**, p. 63–70.

Latimer, R., Davison, R., van Riel, P., 2000, An interpreter's guide to understanding and working with seismic-derived acoustic impedance data: The Leading Edge, no.3, p. 242-256.

Levy, J.H., Stewart, J.D., Killingley, K.S., 1997, Methane capacities of Bowen Basin coals related to coal properties: Fuel, **76**, Issue 9, p. 813-819.

Levy, S., Fullagar, P., 1981, Reconstruction of a sparse spike train from a portion of its spectrum and application to high-resolution deconvolution: Geophysics, **46**, n. 9, p. 1235-1243.

Lindseth, R.O., 1979, Synthetic sonic logs-a process for stratigraphic interpretation: Geophysics, **44**, n. 1, p. 3-26.

Lines, L.R., Newrick, R.T., 2004, Fundamentals of geophysical interpretation: SEG Geophysical Monograph Series No. 13, Society of Exploration Geophysicists.

Mavor, M., Faltinson, J., 2008, Enerplus 102 Pembina 7-28-46-7 W5M, CO_2 Micro-pilot Analysis, Albert Research Council. Confidential report.

McCrank, J., Lawton, D., 2006,Well log study and seismic survey of a coal-bed methane site: Alder Flats, Alberta, CREWES Research Report, **18**.

McCran, J., Lawton, D., 2007, Alder Flats 2D and 3D Seismic Programs, CREWES Sponsors Annual Report 2007.

Oldenburg, D., Scheuer, T., Levy, S., 1983, Recovery of the acoustic impedance from reflection seismograms: Geophysics, **48**, n. 10, p. 1318-1337.

Pana, C., 2007, Ardley Coal Zone Characterization and Coal-Sandstone Channels Architecture, Pembina CBM Exploration Block, Alberta, EUB/AGS Earth Sciences Report 2007-04.

Russell, B., Hampson, D., 1991, Comparison of poststack inversion methods: SEG Expanded Abstracts, SEG Annual Meeting 1991.

Shimada, S., Li, H., Oshima, Y., Adachi, K., 2005, Displacement behaviour of CH4 adsorbed on coals by injecting pure CO2, N2, and CO2-N2 mixture: Environmental Geology, **49**, p. 44-52.

Veeken, P., Da Silva, M., 2004, Seismic inversion methods and some of their constraints: First Break, **22**, p. 47-70.

Viete, D.R., Ranjith, P.G., 2006, The effect of CO2 on the geomechanical and permeability behaviour of brown coal: implications for coal seam CO2 sequestration: International Journal of Coal Geology, **66**, no. 3, p. 204–16.

Viete, D.R., Ranjith, P.G., 2007, The mechanical behaviour of coal with respect to CO_2 sequestration in deep coal seams: Fuel, **86**, 2667-2671

Wang, Z.Z., 2001, Fundamentals of seismic rock physics: Geophysics, **66**, p398-412.